

Homogenization Methods and Multiscale Modeling: Nonlinear Problems

Marc G. D. Geers¹, Varvara G. Kouznetsova¹, Karel Matouš²,
Julien Yvonnet³

¹*Department of Mechanical Engineering, Eindhoven University of Technology, Eindhoven, The Netherlands*

²*Department of Aerospace and Mechanical Engineering, University of Notre Dame, Notre Dame, IN, USA*

³*Laboratoire Modélisation et Simulation Multi Echelle, Université Paris-Est Marne-la-Vallée, France*

1	Introduction	1
2	From Micromechanics to Multiscale Mechanics: Historical Note	2
3	Multiscale Approaches for Nonlinear Problems: Overview	3
4	Multiscale Computational Homogenization	8
5	RVE Aspects and Statistics for Nonlinear Materials	14
6	Decoupled Computational Homogenization Methods	19
7	Parallel Implementations and High-Performance Multiscale Computing	23
8	Concluding Remarks	27
	Acknowledgments	28
	Notes	28
	References	28

1 INTRODUCTION

Modern multiscale methods are rooted in powerful state-of-the-art computational techniques when nonlinearities are involved. Addressing scientific and engineering

questions using scale transitions is one of the most challenging and rewarding routes in solving fundamental problems in materials science and engineering for the next century.

The intrinsic role of different scales in mechanics of materials is nowadays well recognized. At the level of the material, the typical scale that matters is the characteristic scale of the microstructural heterogeneities and defects. The mechanics and physics of these multiphase heterogeneous microstructures is generally considered the main driver for the macroscopic engineering response of a material, including its failure behavior. The proper understanding of the behavior, evolution, and mechanical response of materials at the micro scale is critical. Over time, it has become evident that even smaller scales and thin interfaces may have a pronounced influence on the micron scale. In this sense, multiscale methods have emerged that link smaller and larger scales. A second characteristic of this multidisciplinary field is the emphasis that is put on the mechanical aspects, covering the role of stress, strain, deformation, and degradation. Generally, this goes hand in hand with the material synthesis and microstructure evolution, since internal stress fields are an intrinsic characteristic of heterogeneous microstructures. It is obvious that the character of the intrinsic microstructure cannot be trivially separated from the governing physics. Mechanical aspects generally represent a source of internal (strain) energy, which is an essential ingredient of the underlying thermodynamics. Moreover, other physical mechanisms (e.g., diffusion and dislocation motion) will have a pronounced influence on the relaxation

of these internal stresses, and consequently on the overall mechanical response. Evidently, these phenomena are intrinsically nonlinear in nature, which necessitates proper multiscale computational techniques.

While homogenization of heterogeneous materials was one of the first multiscale approaches in mechanics, it was originally developed for elastic problems, whereby the small scale can often be eliminated in the computational process. For more complex nonlinear problems, this is obviously not the case. Many problems require the explicit solution at multiple scales, whereby an iterative solution process at each scale entails high computational costs. It is this category of problems that is the main focus of the present chapter.

The chapter will start with a brief historical overview, followed by a methodological classification of some popular multiscale methods in mechanics of materials. Separate sections will be devoted to selected methods, that is, nonlinear computational homogenization (CH), statistical aspects of representative volume elements (RVE), decoupled multiscale modeling, (nonlinear) transformation field analysis, and parallel computational implementation in three dimensions.

Cartesian tensors and tensor products will be used throughout this chapter, making use of a Cartesian vector basis $\{\vec{e}_1, \vec{e}_2, \vec{e}_3\}$. Second-order tensors are denoted as \mathbf{A} , whereas fourth-order tensors are written as ${}^4\mathbf{A}$. Using the Einstein summation rule, the following conventions are used in the adopted compact tensor notations:

$$\mathbf{C} = \vec{a} \otimes \vec{b} = a_i b_j \vec{e}_i \otimes \vec{e}_j \quad (1)$$

$$\mathbf{C} = \mathbf{A} \cdot \mathbf{B} = A_{ij} B_{jk} \vec{e}_i \otimes \vec{e}_k \quad (2)$$

$$\mathbf{C} = {}^4\mathbf{A} : \mathbf{B} = A_{ijkl} B_{lk} \vec{e}_i \otimes \vec{e}_j \quad (3)$$

$$c = \mathbf{A} : \mathbf{B} = A_{ij} B_{ji} \quad (4)$$

2 FROM MICROMECHANICS TO MULTISCALE MECHANICS: HISTORICAL NOTE

The grand challenge in multiscale mechanics consists in identifying the relationships that bridge various length scales, including those yielding (emergent) effective/macroscopic properties. Multiscale methods typically aim to extract predictive macroscopic properties of materials by resolving the geometrical and physical details of the underlying microstructure. At the microscale, proper descriptions of the individual phases and interfaces are thereby required. In order to bridge scales, a number of methods have been proposed in the literature. ‘‘Homogenization’’, as defined in the mechanics community, or ‘‘coarse graining’’, as defined

in the physics community (Ridderbos, 2002; Ahuja *et al.*, 2008), is certainly one of the largest classes of multiscale methods. The term ‘‘homogenization’’ was originally coined by Ivo Babuška (1976). Strictly speaking, coarse graining and homogenization are not identical. Homogenization is essentially based on averaging theorems, whereas coarse graining in physics relies on statistical mechanics or thermodynamics in view of identifying the emergent behavior across the scales. In the latter category, the GENERIC framework (Öttinger, 2005; Hütter and Tervoort, 2008a,b; Grmela, 2010a,b) is particularly worth mentioning. Physicists often make use of renormalization tools to establish a coarse-grained picture of complex multiscale phenomena.

Early steps in homogenization were taken long ago, when the interest for the micromechanics of heterogeneous materials became more pronounced. Preliminary developments go back to the nineteenth century, where the rule of mixtures was first introduced (Voigt, 1887), followed by the Sachs model (Sachs, 1928), Reuss estimate (1929), and the frequently used Taylor model (Taylor, 1938). While Voigt and Reuss estimates were typically used for composite systems, Taylor and Sachs models were derived for polycrystals. The growing interest in composite materials constituted the main motivation for stronger developments in homogenization. The best-known early contribution is probably the work of Eshelby (1957), where attention was given to the elastic solution for an ellipsoidal inclusion. Still today, these first steps have had a pronounced impact, giving rise to alternative continuum mechanics frameworks (Eshelbian mechanics and materials forces). One of the essential characteristics of the micromechanical approaches adopted at that time was the use of continuum mechanics at the scale of the heterogeneities in order to deduce macroscopic constitutive equations. This is what characterizes ‘‘continuum micromechanics’’, a field that has been extended tremendously since then. This field was formally established by Hill (1965), who was undoubtedly one of the main contributors. A survey of activities over the past 40 years is given in Zaoui (2002).

The period of 1950–1980 is characterized by the major progress made in the homogenization of heterogeneous elastic solids, which is given particular attention in **Homogenization Methods and Multiscale Modeling**. Pioneering work in this timeframe was done by Kröner (1958), Hashin and Shtrikman (1963), Hill (1963), Mori and Tanaka (1973), Babuška (1977), and Willis (1977), among others. First steps toward an extension into the nonlinear regime of the already developed elastic homogenization theories, and variational principles were taken by a few authors in this period (Kröner, 1961; Hill, 1965; Hutchinson, 1976), whereas many more papers on the subject appeared

in the 1980s and 1990s. Treated subjects include elastoplasticity (both rate-independent and viscoplastic), nonlinear elasticity, and viscoelasticity. Frequently cited contributors in this field are Nemat-Nasser and Obata (1986), Nemat-Nasser and Hori (1993), Ponte Castañeda (1991), Suquet (1993, 1997a), Willis (1994), and Zaoui and Masson (2000), among others.

Different applications in the nonlinear range appeared in the late 1970s, for example, by the well-known Gurson model (Gurson, 1977) for void growth in ductile materials, which gave rise to more papers on the plasticity of porous materials. Multiscale mechanics was considered as a natural tool that allowed to study the influence of the mechanics at a microlevel (deformation and failure) on the macroscopic material behavior. The main interest at that time consisted in the derivation of macroscopic constitutive equations that implicitly incorporate the microscale deformation mechanisms. Making appropriate assumptions, analyses were made for grain effects (grain–grain interaction, grain size, and grain orientation/texture), inclusions/particles distributed in a hard or soft matrix with various interfaces, voids (nucleation, growth, and coalescence), microcracks, fiber–matrix systems, and so on. Most of the attention, however, was given to creep, (visco) plasticity, damage, and fracture.

The developments in mathematical homogenization have been key in nucleating the engineering applications of homogenization. This was already (partially) addressed the Chapter on **Homogenization Methods and Multiscale Modeling**, focusing on linear problems. In this context, the contributions of Keller (1964, 1977), Benssousan *et al.* (1978), Lions (1979) were pioneering. The follow-up work of Sanchez-Palencia (1980) served as an impetus for researchers in computational mechanics. Duvaut (1979) and Suquet (1987) devoted themselves to the study on the theory of homogenization within the framework of mechanics of heterogeneous or composite materials, which has triggered various engineering applications with numerical simulation results. Once the common ground between mathematical homogenization and engineering was found, the homogenization method began to prevail in the area of computational mechanics. Supported by advanced computational solution methods, the homogenization method has become a common tool to characterize the mechanical or various physical properties of heterogeneous media with (periodic) microstructures and is now known as one of the rigorous theoretical backgrounds for (nonlinear) CH. Since the 1990s, the steady increase of available computational power has led to a strongly developed computational discipline in multiscale mechanics. Many achievements have been made since then, and many more may be expected in the (near) future.

3 MULTISCALE APPROACHES FOR NONLINEAR PROBLEMS: OVERVIEW

Multiscale modeling of nonlinear material behavior is a vast subject, whereby it is almost impossible to give a complete overview of all methods that have been developed in the past. Instead, a succinct overview will be given here, with special emphasis on a few selected methods that will be detailed further in this chapter. The targeted application area considered here is the upscaling of the nonlinear mechanical response of heterogeneous materials.

3.1 General classification

There is no unique classification that unifies all multiscale methods presently available. From a methodological perspective, different categories of multiscale methods can be identified, (Weinan *et al.*, 2007; Weinan, 2011; Fish, 2006, 2009), related to the location and geometry of the heterogeneous scale. One category concerns problems that have isolated details (e.g., defects and cracks) that need to be resolved with a high resolution and accuracy. The fine scale problem is then limited to a small part of the global domain. This type of problem is often also labeled as “multiple scales” rather than multiscale. Another category concerns problems where the macroscopic response has to be extracted from the underlying fine scale behavior in large parts of the domain, whereby the fine scale will be probed to determine the effective macroscopic response. The third category concerns mixed problems, combining the two previous categories. The last category identified by Weinan *et al.* (2007) are problems revealing self-similarity across the scales, which will not be further explored here.

Different classifications of multiscale methods have been proposed in the literature. For a more complete overview, see, for example, Fish (2006, 2009). A frequently used classification of multiscale methods is based on the underlying *problem formulation* (continuum or discrete):

- *Concurrent methods*: In concurrent methods, both scales are simultaneously addressed in the problem formulation. In general, different length and time scales can be used in a single domain and different methodologies may be used on different parts of the domain. In practice, the name “concurrent” is often restricted to methods where different scales (and methodologies) are used in different parts of the domain (Fish, 2006).
- *Hierarchical methods*: In hierarchical methods, the scales are linked in a hierarchical manner, which implies that distinct scales are considered and coupled in the same part of a domain. The hierarchical link may be

established through, for example, volume averaging of field variables or just simple parameter identification.

- *Hybrid methods:* Hybrid methods typically reveal properties of different classes, for example, multigrid methods (Miehe and Bayreuther, 2007), generalized finite element method (Plews and Duarte, 2014), wavelet-based methods, and quasi-continuum methods (Tadmor *et al.*, 1996a).

Multiscale methods can also be classified from an *algorithmic* perspective, referring to the actual solution procedure:

- *Parallel methods:* Parallel methods solve both scales in parallel (or in a monolithic manner). They are therefore coupled in that sense.
- *Serial or sequential methods:* Serial methods rely on a serial algorithm to solve and couple both scales. Scales are typically linked through data passing, whereby each scale is solved separately. This solution procedure naturally fits hierarchical multiscale problems.
- *Coupled or decoupled methods:* In many cases, the solution procedure can be set up in either a coupled or decoupled manner. In a coupled scheme, the solution of both scales is computed and coupled in an on-line manner. In a decoupled scheme, one of the scales is computed beforehand, through prior off-line computations.

Among the multiscale methods listed above, particular attention will be given to CH methods. This method is typically hierarchical, even though the solution method for the fully coupled nonlinear problem is more parallel than serial (the iterative solution processes are imbricated, that is, equilibrium at both scales is established simultaneously). These methods are essentially based on the integration over small length scales (e.g., over a microstructural RVE).

Variational multiscale methods (Hughes *et al.*, 1998; Garikipati and Hughes, 2000) constitute a particular category of hierarchical techniques. This category relies on the weak form of the governing equations, which are split into a fine scale and a coarse scale contribution. The problem needs to be complemented by suitable assumptions on the fine scale field, which play an important role in the efficiency and physical relevance of the method. The fine scale is generally eliminated from the resulting formulations, which may entail quite severe restrictions. Classical fine scale fluctuations, like displacement discontinuities, can be adequately addressed. For this particular case, a close resemblance with the extended finite element method emerges (Moës and Belytschko, 2002).

Multiscale methods are used in different communities, with a different emphasis and often also a different terminology.

While this chapter focuses on its application to mechanics of materials, it is worth noting that a vast amount of literature exists in the physics and mathematics community, see the book of Weinan (2011) for an overview. The heterogeneous multiscale method (HMM; Weinan *et al.*, 2007; Abdulle *et al.*, 2012) is often used in the computational mathematics oriented literature, but it shares many common characteristics with the CH method detailed further on in this chapter.

In the following sections, explicit emphasis is given to methods used for upscaling the nonlinear mechanical response of materials.

3.2 Material nonlinearities and fine scale methods

Nonlinear homogenization methods have wide ranging application to many natural and manufactured materials: asphalt, bone, ceramics, composites, concrete, geological materials and granular media, glass, metals, paper, polymers, rock, snow, ice, textile, biological tissues, and so on. At small scales, nonlinear phenomena are the rule rather than the exception. Plasticity, crack nucleation and propagation, defect mechanics (e.g., dislocations), phase transformations, inelastic creep and relaxation, and microstructure evolution in general are the prime drivers for the occurring nonlinearities (Nemat-Nasser, 1992; Ortiz, 1996; Tvergaard, 1997; Zaoui, 2002).

Composites have attracted such a large interest that they are worth mentioning as a field on their own. Driven by an engineering interest, a lot of attention has been given to matrix–fiber systems, covering the elastic range, the nonlinear range, interfacial aspects, geometrical aspects (isotropic and anisotropic configurations), damage, fracture, and so on. Many unit cell and RVE analyses have been made on a variety of fiber–matrix combinations.

Scale transitions in damage and fracture constitute one of the most complex subjects in multiscale mechanics. Damage is a typical phenomenon that develops across all length scales. Many aspects are not well understood, which is reflected in the excessive phenomenological character of most engineering models available. While it has been shown that nonlocality plays an intrinsic role in damage evolution, there is no quantitative or qualitative method available yet for the derivation of a proper (homogenized) nonlocal kernel along with the (homogenized) internal variables. Meanwhile, damage and fracture are more commonly being modeled at the submicron scale and smaller, for example, through atomistics or (polymer) network deformation and failure mechanisms. Incorporating localization and fracture (discontinuities) in a multiscale setting violates the classical principle of scale separation, which disables the application of most classical homogenization methods. Solutions for this require the

explicit incorporation of fine scale kinematics at the coarse scale level.

Any multiscale method critically depends on the modeling accuracy at the smallest scale examined. Multiscale mechanics therefore constitutes a natural bridge to materials science, where the physical characterization and synthesis of microstructures is of prime interest. Capturing the various microstructural deformation mechanisms, ranging from the nanomechanical level to the microstructural entities, is therefore becoming integral part of modern multiscale mechanics. Nonlinear continuum models of complete heterogeneous microstructures are often used for this purpose. However, there are also various examples that depart from the nanoscale to extract aspects relevant for the microscale level. Such techniques are traditionally considered as being part of computational materials science (Raabe, 1998), but the precise differences with computational multiscale micromechanics have not been clearly defined thus far. Among the techniques used in computational materials science, a few extensively used ones are briefly addressed, see Liu *et al.* (2004) for a more extensive overview and Raabe (1998) for more detailed treatments:

- *Monte Carlo methods*: The Monte Carlo method provides approximate solutions to a variety of mathematical problems by performing statistical sampling experiments on a computer. The method applies to problems with no probabilistic content and those with inherent probabilistic structure. They are typically used to formulate a probabilistic equivalent of the physical problem under consideration, which is done by formulating integral expressions of the governing differential equations of the stochastic process. The Monte Carlo algorithm then solves the problem by integrating these expressions using a (weighted) random sampling method. This step is generally computationally expensive. The result of the simulation is obtained by extracting the state equation values, correlation functions, kinetics, and so on. Various types of Monte Carlo methods exist, depending on the sampling method used, the spatial lattice considered, the spin model applied (for lattice type materials in which the flip of particle spins varies the energy), and the energy operator defined. Applications of Monte Carlo methods can be found for a variety of physical phenomena and materials. Applications interesting for mechanics are diffusion, fracture, interfaces, and phase transformations. References are given extensively in Raabe (1998), Binder and Heermann (1998).
- *Molecular dynamics*: This technique is used to model elementary path-dependent processes by solving the equations of motion for all particles (atoms) at an

atomistic scale. Potential functions are used to approximate the atomic interactions, in combination with the classical equation of motion. These potentials range in complexity, from simple pair potentials to many-body potentials, where the number of neighboring atoms is gradually augmented in the interactions. Classical pair potentials consider nearest-neighbor interaction only (Lennard-Jones, Morse, and Torrens), see Torrens (1972) and Vitek (1996) for more details. Applications of molecular dynamics relevant for micromechanics are dislocations, microcracks, thin films, surfaces, interfaces, and so on. The interested reader is again referred to Raabe (1998) for an overview and references in each of these fields. One of the main limitations of this method is the size of the system that can be resolved, since, for example, the use of all lattice degrees of freedom in a crystalline material clearly limits the number of atoms that can be taken into account. Moreover, the analysis typically spans very short timescales only. From a molecular dynamics simulation, macroscopic properties of a system are explored through microscopic simulations, for example, to calculate changes in the binding free energy of a particular drug candidate or to examine the energetics and mechanisms of conformational change. The connection between microscopic simulations and macroscopic properties is made via statistical mechanics (Chandler, 1987; Wilde and Singh, 1998), which provides the rigorous mathematical expressions that relate macroscopic properties to the distribution and motion of the atoms and molecules. Molecular dynamics simulations enable the evaluation of these mathematical formulas. As a result, thermodynamic properties and/or time-dependent (kinetic) phenomena can be studied. Note that a more generalized framework is given under the name “Particle Dynamics Method”.

- *Quasi-continuum methods*: These approaches typically bridge atomistic models to continuum approaches, where multiple scales are considered simultaneously (Tadmor *et al.*, 1996a,b; Knap and Ortiz, 2001; Curtin and Miller, 2003). Direct atomistic calculations are thereby often used as the source for the constitutive input. Quasi-continuum methods have also been extended to address fibrous network-based materials, as well as dissipative processes, see Beex *et al.* (2014a,b).

3.3 Nonlinear homogenization of materials

As emphasized in the historical note, multiscale mechanics is rooted in the analysis of the homogenized response of heterogeneous elastic materials. Homogenization frameworks focus on the equivalent or effective response of a

finite volume of material, which is generally assumed to be statistically homogeneous. Characteristic volumes were identified as unit cells for periodic materials and RVEs (Hill, 1963; Drugan and Willis, 1996) for statistically heterogeneous media (see Section 5 for more details). The response of such a volume is assumed to be equivalent to the response of the homogeneous equivalent continuum (HEC), for which the continuum mechanics response is solved. Originating from the statistical mechanics community, the concept of a representative unit cell (RUC) is frequently used as well, rather than an RVE. The definition of an RUC essentially relies on statistical descriptors, and hence the morphology approximation error is better defined from a quantitative perspective (Povirk, 1995; Kumar *et al.*, 2006, 2008; Lee *et al.*, 2009). Throughout the literature, both RVE and RUC are used, whereby the difference is generally not made explicit. RVE concepts essentially rely on the principle of *separation of scales*. This principle states that the scale of the microstructure or microstructure fluctuation, ℓ_μ , must be smaller than the size of the representative volume considered, ℓ_m , which must be much smaller than the characteristic fluctuation length in the macroscopic deformation field, ℓ_M .

$$\ell_\mu < \ell_m \ll \ell_M \quad (5)$$

Following this definition, the absolute size of the macrostructure is not relevant for this scale separation. While this principle is valid within the continuum mechanics concept of local action, it is sometimes violated when either a microstructural length scale tends to be large (e.g., in the presence of long-range correlations or percolation phenomena) or when the scale of the macroscopic (strain) fluctuations tends to be small (e.g., localization of deformation and gradients).

Homogenization techniques (first developed for elasticity) have been extended toward higher order and nonlocal constitutive equations in the past two decades, for example, developments include Cosserat media (Forest *et al.*, 2001), couple stress theory (Smyshlyaev and Fleck, 1994), nonlocal effective continua (Drugan and Willis, 1996), or higher order gradient homogenized elastic materials (Triantafyllidis and Bardenhagen, 1996; Smyshlyaev and Cherednichenko, 2000; Peerlings and Fleck, 2001). Other interesting approaches toward the analysis of random (physically nonlinear) microstructures (Ponte Castañeda, 1992, 2002; Suquet, 1993) are the Taylor–Bishop–Hill estimates, several generalizations of self-consistent schemes, and asymptotic procedures (Fish *et al.*, 1997). Homogenization of solids accounting for both geometric and material nonlinearity is clearly more demanding. Interesting contributions are given and cited in Doghri and Friebel (2005). Mean-field methods for nonlinear materials have been addressed in Doghri

et al. (2011). Homogenization estimates for nonlinear composites are presented in Agoras and Ponte Castañeda (2011). Homogenization-based constitutive models have been proposed for magnetorheological elastomers at finite strains in Ponte Castañeda and Galipeau (2011). Mathematical or asymptotic homogenization approaches for nonlinear material behavior have been elaborated in several papers, for example, Fish and Fan (2008), Markenscoff and Dascalu (2012), Yang *et al.* (2013).

Several analyses have been performed on unit cells, from which the parameters in assumed macroscopic constitutive equations can be assessed. Some of them also include higher order continuum formulations, for example, Cosserat (van der Sluis *et al.*, 1999) and couple stress media (Ostoja-Starzewski *et al.*, 1999). The added value of these multiscale methods depends on the accuracy (geometrical, physical, and mechanical) with which the microstructure is modeled, as well as the technique that is used to perform the homogenization toward the macroscopic level. Closed-form homogenization toward constitutive material frameworks or effective (or rather apparent) material properties of composites turns out to be really cumbersome if one wishes to take into account more complex physics, geometrical nonlinearities, or damage and/or localization.

3.4 Nonlinear computational homogenization

In the past decade, substantial progress has been made in the two-scale CH of complex multiphase solids (Geers *et al.*, 2010). This method is essentially based on the nested solution of two boundary value problems, one at each scale. Though computationally expensive, the procedures developed allow to assess the macroscopic influence of microstructural parameters in a rather straightforward manner. The first-order technique is by now well established and widely used in the scientific and engineering community (Suquet, 1985a; Ghosh *et al.*, 1996, 2001; Smit *et al.*, 1998; Miehe *et al.*, 1999a,b; Feyel and Chaboche, 2000; Terada *et al.*, 2000; Kouznetsova *et al.*, 2001; Terada and Kikuchi, 2001; Miehe and Koch, 2002). Since the late 1990s, many contributions of CH methods were developed for, for example, porous media (Ehlers *et al.*, 2003), cellular materials (Ebinger *et al.*, 2005), polycrystalline metals, and granular materials. Many of these focused on linear problems, and for compactness we restrict this overview to nonlinear problems that have been resolved since then.

Making additional hypotheses on the averaging of microscale fields and the virtual power statement between scales, several extensions have been proposed in the literature:

- *Higher order CH*: This scheme makes use of an enriched description of the macroscale kinematics, which is used to construct a more complex microscale problem. The homogenization allows to extract the Cauchy stress tensor, along with higher order stress tensor and all accompanying tangents (Geers *et al.*, 2001, 2003; Kouznetsova *et al.*, 2002, 2004a,b; Kouznetsova, 2002; Kaczmarczyk *et al.*, 2008, 2010; Bacigalupo and Gambarotta, 2011). The computational continua approach (Fish and Kuznetsov, 2010; Fish *et al.*, 2015) is a variant that relaxes the constraints on higher order continuity and boundary conditions.
 - *Continuous–discontinuous homogenization–localization*: Incorporating the transition from damage to fracture (via localization) in a multiscale approach is a real challenge (Loehnert and Belytschko, 2007; Belytschko *et al.*, 2008; Hettich *et al.*, 2008). The recently developed methods of this type rely on an adequate solution for the lack of scale separation between both scales (i.e., by taking microscale kinematics explicitly on board at the macro scale). Localized properties at the microscale have to be incorporated directly in the macroscale description without any averaging. Solutions have been proposed in which a discrete band (weak discontinuity) is used at the macroscale (Massart *et al.*, 2007a,b), as well as a discontinuous jump (strong discontinuity) at the macroscale (Coenen *et al.*, 2012a,b; Bosco *et al.*, 2014, 2015). In each case, the fine scale is modeled as a regular continuum, with appropriate regularized damage or plasticity models. The coarse scale is enriched, for which embedded discontinuities or X-FEM (extended finite element method)-based solution algorithms have been used. Note that simplified approaches have been proposed to make a direct volumetric coupling between the size of a finite element (at the macroscale) and the localizing RVE at the microscale (Gitman *et al.*, 2008). In contrast to the previously cited methods, this solution is not really of the homogenization type anymore and rather resembles a domain decomposition approach in which the fine scale is embedded as a local refinement.
 - *Geometrical microstructural instabilities*: Another case that violates scale separation is induced by local (buckling) instabilities at the level of the microstructure, as typically encountered in cellular materials. This received particular attention in the work of (Miehe *et al.*, 2002), and more recently in (Nezamabadi *et al.*, 2009).
 - *Thermomechanical CH*: This scheme is a coupled problem, providing the homogenization of coupled thermal and mechanical processes (Özdemir *et al.*, 2008a,b).
 - *Substructured thin sheets and shells*: CH applied to beams, plates, and shells makes use of the higher order kinematics already developed for the second-order scheme. The RVEs are homogenized in the (shell) plane and integrated through their thickness. This method enables nonlinear CH for shell-type continua (Geers *et al.*, 2007; Coenen *et al.*, 2010; Cong *et al.*, 2015).
 - *Multiscale interfaces or cohesive cracks*: CH of interfaces typically couples a cohesive zone type description at the macroscale to an interfacial RVE at the microscale (Matouš *et al.*, 2008; Verhoosel *et al.*, 2010; Nguyen *et al.*, 2012; Mosby and Matouš, 2015a).
 - *Multiphysics problems*: CH has been extended toward other (coupled) fields, for example, electromagnetism (Javili *et al.*, 2013; Zäh and Miehe, 2013; Niyonzima *et al.*, 2014; Keip *et al.*, 2014), diffusion problems (Nilenius *et al.*, 2014), liquid-phase sintering (Ohman *et al.*, 2013), heat flow (Larsson *et al.*, 2010), or involving chemical couplings (Yuan *et al.*, 2014).
 - *Contact and friction problems*: Contact and friction at the small scale always involves rough surfaces, for which a CH approach is naturally versatile (De Lorenzis and Wriggers, 2013; Temizer, 2014a).
 - *Dynamics of materials*: Extending the scheme to incorporate the dynamics of propagating waves and microinertia has been carried out in Pham *et al.* (2013). This method allows the analysis of nonlinear wave transmission and attenuation phenomena, whereby local resonance effects inside the microstructure are incorporated. Typical examples of interest are locally resonant acoustic metamaterials.
- In recent years, the number of contributions that further developed CH methods or made use of it for the multiscale analysis of materials steadily increased. Among others, various applications can, for example, be found in the following:
- porous media, for example, Su *et al.* (2011) and Zhuang *et al.* (2015)
 - cellular materials, for example, Nguyen and Noels (2014) and Ilchev *et al.* (2015)
 - soft matter, for example, Temizer (2014b)
 - polycrystalline metals, for example, Segurado and Llorca (2013)
 - technical textiles, for example, Fillep *et al.* (2015)
 - granular materials, for example, Liu *et al.* (2014)
 - trabecular bone, for example, Wierszycki *et al.* (2014)
 - composite plates, for example, Helfen and Diebels (2014)
 - Li-ion battery cells, for example, Salvadori *et al.* (2014)
- While CH is an extremely powerful multiscale technique, it comes along with a high computational cost. Nevertheless,

CH is naturally parallelizable (Mosby and Matouš, 2015a) and the method has demonstrated excellent scalability as shown later in this chapter. Alternatively, a growing emphasis is given on its efficiency, whereby use is made of advanced computational techniques and reduced order models (Yvonnet and He, 2007; Fritzen and Leuschner, 2013; Fritzen *et al.*, 2014; Kerfriden *et al.*, 2014).

3.5 Nonuniform transformation field analysis

Part of this chapter on nonlinear multiscale methods is devoted to the (nonuniform) transformation field analysis ((N)TFA). The TFA method was originally proposed by Dvorak (1992) for inelastic composite materials, using piecewise uniform transformation fields. The method typically approximates the stress or strain field as uniform in each phase of a heterogeneous microstructure. On that basis, the overall homogenized properties of a heterogeneous RVE can be estimated. The extension to NTFA followed in the work of Michel and Suquet (2003). The homogenization of nonlinear heterogeneous materials on the basis of the NTFA method has been studied more extensively in the past decade, see, for example, the work of Roussette *et al.* (2009), Fritzen and Boehlke (2011), Fritzen and Leuschner (2013). A variant of the TFA approach for inelastic materials is also proposed in Fish *et al.* (2013). In the context of more efficient multiscale schemes, the NTFA method is certainly important.

4 MULTISCALE COMPUTATIONAL HOMOGENIZATION

In this section, the main principles of the classical (first-order) CH are briefly summarized. First, CH for mechanical problems will be detailed, followed by the general guidelines for problems involving other fields, for example, thermal, electric, magnetic, and the coupled fields.

4.1 Macroscale problem

Consider a microscopically heterogeneous body, subjected to loading and constraints, such that the separation of scales principle (see inequality (5)) is respected. At the macroscopic scale, the motion is governed by the momentum balance, in the absence of body forces, expressed as

$$\vec{\nabla}_{0M} \cdot \mathbf{P}_M^T = \rho_{0M} \ddot{\vec{x}}_M \quad (6)$$

supplemented by initial and boundary conditions. In (6), \mathbf{P}_M is the first Piola–Kirchhoff stress tensor; $\vec{\nabla}_{0M}$ is the gradient operator with respect to the reference configuration; \vec{x}_M and

$\vec{\bar{X}}_M$ denote the position vectors in the current and reference configurations, respectively; $\ddot{\vec{x}}_M$ is the acceleration; the superscript “T” denotes transposition; and the subscript “M” refers to a macroscale quantity, while the subscript “m” will denote a microscale quantity. Under the assumption of the full-scale separation, also known as the long-wave approximation, the macroscopic effective density in the reference configuration ρ_{0M} can be computed simply as the weighted average of the densities of the microstructural constituents (Sanchez-Palencia, 1980).

To close this boundary value problem, a constitutive relation between the stress and kinematical quantities needs to be postulated. Instead of assuming a constitutive equation in a closed form, the CH technique extracts the constitutive response numerically from the detailed computational analysis of a microstructural RVE.

The CH framework is schematically illustrated in Figure 1. The macroscopic deformation (gradient) tensor \mathbf{F}_M is calculated for every material point of the macrostructure (e.g., the integration points of the macroscopic mesh within a finite element environment). Next, \mathbf{F}_M is used to formulate the boundary conditions imposed on the RVE that is assigned to this point. Upon the solution of the boundary value problem for the RVE, the macroscopic stress tensor \mathbf{P}_M is obtained, thus providing the numerical stress–deformation relationship at the macroscopic point. The local macroscopic consistent tangent 4C_M , which is needed for the iterative solution of the macroscopic nonlinear problem, is also derived from the microstructural analysis.

Next, the microscale boundary value problem will be formulated based on the scale transition relations, followed by the details of its numerical implementation.

4.2 Microscale problem

The physical and geometrical properties of the microstructure are identified by an RVE. The proper selection of the RVE is a rather delicate task and will be treated in detail in Section 5. Here, it is assumed that an appropriate RVE, capable of capturing relevant microscale physics and fluctuations, has already been selected. In accordance with the separation of scales principle, the RVE should be much smaller than the characteristic length of the relevant macroscopic field variation, but sufficiently larger than microfluctuations. If this condition holds, then any change in the macroscopic field variables will immediately be accommodated at the RVE scale, that is, the RVE problem is quasi-static even though the macroscopic problem can be transient.

The classical first-order CH departs from the linearization of the macroscopic nonlinear deformation map, given by the macroscopic deformation gradient tensor $\mathbf{F}_M = (\vec{\nabla}_{0M} \vec{x}_M)^T$.

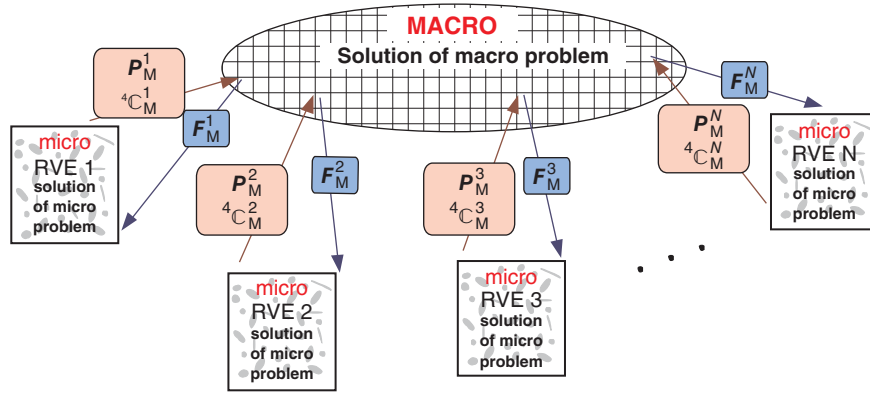


Figure 1. Computational homogenization scheme.

A material vector $\Delta \vec{x}_m$ in the current configuration of the RVE can be related to the same material vector $\Delta \vec{X}_m$ in the reference configuration as

$$\Delta \vec{x}_m = \mathbf{F}_M \cdot \Delta \vec{X}_m + \vec{w}_m \quad (7)$$

where $\Delta \vec{x}_m = \vec{x}_m - \vec{x}_m^c$ and $\Delta \vec{X}_m = \vec{X}_m - \vec{X}_m^c$ are relative position vectors with respect to an arbitrary reference point. The first term in (7) expresses the homogeneous deformation given by \mathbf{F}_M , while the microfluctuation field \vec{w}_m is identified as the local fine scale contribution superimposed on to the macroscale deformation.

The RVE deformation is described by the microstructural deformation gradient tensor $\mathbf{F}_m = (\vec{\nabla}_{0m} \vec{x}_m)^T$, where the gradient operator $\vec{\nabla}_{0m}$ is taken with respect to the reference microstructural configuration. From (7), the microscale deformation gradient tensor \mathbf{F}_m is determined as

$$\mathbf{F}_m = (\vec{\nabla}_{0m} \vec{x}_m)^T = \mathbf{F}_M + (\vec{\nabla}_{0m} \vec{w}_m)^T \quad (8)$$

Relations (7) and (8) are valid for every point at the microscale, with the first terms readily known for a given macroscale deformation tensor \mathbf{F}_M . The microfluctuation \vec{w}_m will follow from the solution of the microscale boundary value problem.

As stated above, the microscale boundary value problem is quasi-static. In the absence of body forces, the equilibrium equation for the RVE in terms of the microscale first Piola–Kirchhoff stress tensor \mathbf{P}_m is written as

$$\vec{\nabla}_{0m} \cdot \mathbf{P}_m^T = \vec{0} \quad (9)$$

The material behavior of each microstructural constituent α (e.g., matrix, inclusion, and interphase) is assumed to be known and described by constitutive laws that specify a time-

and history-dependent stress–strain relationship, possibly involving microstructural evolution,

$$\mathbf{P}_m^{(\alpha)}(t) = \mathcal{F}_p^{(\alpha)} \{ \mathbf{F}_m^{(\alpha)}(\tau), \tau \in [0, t] \} \quad (10)$$

where t denotes the current time.

The microscopic equilibrium equation (9) requires boundary conditions. The essential step in the CH methodology is the derivation of RVE boundary conditions from the scale transition relations, as is discussed in the following.

4.3 Scale transition relations

4.3.1 Macro-to-micro: kinematics

One of the most commonly used scale transition relations to establish the macro-to-micro coupling is the kinematical averaging relation. It requires the volume average of the microscale deformation gradient tensor \mathbf{F}_m to be equal to the corresponding macroscale deformation gradient tensor \mathbf{F}_M , that is,

$$\mathbf{F}_M = \frac{1}{V_{0m}} \int_{V_{0m}} \mathbf{F}_m \, dV_{0m} \quad (11)$$

where V_{0m} is the RVE volume in the reference configuration. Insertion of equation (8) into the right-hand side of the scale transition relation (11) yields

$$\begin{aligned} \frac{1}{V_{0m}} \int_{V_{0m}} \mathbf{F}_m \, dV_{0m} &= \mathbf{F}_M + \frac{1}{V_{0m}} \int_{V_{0m}} (\vec{\nabla}_{0m} \vec{w}_m)^T \, dV_{0m} \\ &= \mathbf{F}_M + \frac{1}{V_{0m}} \int_{\Gamma_{0m}} \vec{w}_m \otimes \vec{N}_m \, d\Gamma_{0m} \end{aligned} \quad (12)$$

where the divergence theorem has been used to transform the volume integral to an integral over the undeformed boundary of the RVE, Γ_{0m} , with outward normal \vec{N}_m .

It is immediately clear that the boundary conditions on the RVE must be chosen such that the contribution of the microfluctuation field \vec{w}_m into equation (12) vanishes in order to satisfy the scale transition relation (11). This can be achieved in many alternative ways. Some of the possibilities proposed and used in the literature are listed below:

1. Do not allow for any microstructural fluctuations within the RVE, that is,

$$\vec{w}_m = \vec{0}, \quad \forall \vec{X}_m \in V_{0m} \quad (13)$$

enforcing the entire volume to deform according to the prescribed \mathbf{F}_M , that is,

$$\mathbf{F}_m = \mathbf{F}_M, \quad \forall \vec{X}_m \in V_{0m} \quad (14)$$

In the literature, this is usually referred to as the *Taylor (or Voigt) assumption*.

2. Suppress the microfluctuation at the RVE boundary only

$$\vec{w}_m = \vec{0}, \quad \forall \vec{X}_m \in \Gamma_{0m} \quad (15)$$

while leaving the microstructural fluctuations inside the volume yet undetermined. Using equation (7), the above relation can equivalently be written as

$$\Delta \vec{x}_m = \mathbf{F}_M \cdot \Delta \vec{X}_m, \quad \forall \vec{X}_m \in \Gamma_{0m} \quad (16)$$

With this condition, the displacements of the RVE boundary are fully prescribed according to the given \mathbf{F}_M . These are often termed *uniform displacement boundary conditions*.

3. For an RVE with geometrically periodic boundary (e.g., the one sketched in Figure 2), the boundary can be split in “+” and “-” parts defined by the opposite outward normal vectors at the corresponding points, $\vec{N}_m^+ = -\vec{N}_m^-$, and the so-called *periodic boundary conditions* can be imposed by requiring the periodicity of the microfluctuation field

$$\vec{w}_m^+ = \vec{w}_m^- \quad (17)$$

Equivalently, by applying the expression (7) to the material vectors connecting the (arbitrary) reference point and the points on the corresponding “+” and “-” parts of the boundary and subtracting the results leads to the formulation of the periodic boundary conditions in terms of the position vectors of the boundary points

$$\vec{x}_m^+ - \vec{x}_m^- = \mathbf{F}_M \cdot (\vec{X}_m^+ - \vec{X}_m^-) \quad (18)$$

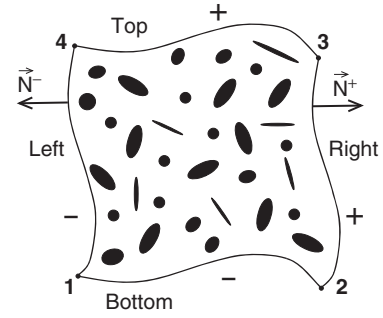


Figure 2. Schematic picture of a two-dimensional RVE.

4. The weakest possible constraint is to require the boundary integral to vanish as a whole

$$\int_{\Gamma_{0m}} \vec{w}_m \otimes \vec{N}_m \, d\Gamma_{0m} = \mathbf{0} \quad (19)$$

In the literature this constraint is sometimes called *minimal kinematic boundary conditions* (Mesarovic and Padbidri, 2005).

Two other simple strategies sometimes used in the literature, which, however, do not directly fit in the kinematics-driven macro–micro scale transition, are:

5. Assume an identical constant stress (and additionally identical rotation) in all microstructural components

$$\mathbf{P}_m = \mathbf{P}_M, \quad \forall \vec{X}_m \in V_{0m} \quad (20)$$

This is called the *Sachs (or Reuss) assumption*.

6. Prescribe tractions on the RVE boundary according to a given macroscopic stress \mathbf{P}_M

$$\vec{p}_m = \mathbf{P}_M \cdot \vec{N}_m, \quad \forall \vec{X}_m \in \Gamma_{0m} \quad (21)$$

These are usually called *uniform traction boundary conditions*.

Of the above choices, the Taylor (Voigt), Sachs (Reuss), and intermediate procedures, where the Taylor or Sachs assumptions are applied complimentary to certain components of the deformation and stress tensors (e.g., in-plane and out-of-plane components for laminated structures), are the most computationally efficient, since they do not require detailed modeling of the microstructure. Accordingly, they generally provide very stiff (Taylor) or very compliant (Sachs) estimates of the overall material properties. Nevertheless, the Taylor and Sachs averaging procedures can be used to quickly obtain a first rough estimate of a composite’s

overall stiffness. The Taylor assumption and some intermediate procedures are often employed in polycrystal plasticity modeling.

The other alternatives to enforce boundary conditions require the solution of the RVE boundary value problem, while allowing the incorporation of local microstructural details. The apparent overall properties obtained by application of uniform displacement boundary conditions on a microstructural cell usually overestimate the effective properties, while the minimal kinematic boundary conditions and uniform traction boundary conditions lead to the underestimation. Moreover, the two latter types of boundary conditions are usually very sensitive to particular microstructural details near the RVE boundary, for example, weak spots (Inglis *et al.*, 2008). For a given microstructural cell size, the periodic boundary conditions are known to provide a better estimation of the overall properties than the other mentioned alternatives (van der Sluis *et al.*, 2000; Terada *et al.*, 2000; Miehe, 2002; Kanit *et al.*, 2003, 2006; Khisaeva and Ostoja-Starzewski, 2006; Perić *et al.*, 2011). The periodic boundary conditions are the most frequently used in practice, although the uniform displacement boundary conditions are also often used, mostly owing to the simplicity of their implementation. Recently, advanced types of RVE boundary conditions have been developed based on combinations of the above boundary conditions designed for specific problems, for example, strain localization (Larsson *et al.*, 2011; Coenen *et al.*, 2012c).

4.4 Micro-to-macro: Hill–Mandel condition

The micro-to-macro scale transition relation is usually established based on the so-called *Hill–Mandel condition* or *macrohomogeneity condition* (Hill, 1963; Suquet, 1985b). This condition requires the volume average of the increment (or variation) of work performed on the RVE to be equal to the increment (or variation) of local work on the macroscale. Formulated in terms of a work conjugated set, that is, the deformation gradient tensor and the first Piola–Kirchhoff stress tensor, the Hill–Mandel condition reads

$$\frac{1}{V_{0m}} \int_{V_{0m}} \mathbf{P}_m : \delta \mathbf{F}_m^T dV_{0m} = \mathbf{P}_M : \delta \mathbf{F}_M^T \quad (22)$$

Using the chain rule, while accounting for the microstructural equilibrium (9),

$$\begin{aligned} \mathbf{P}_m : \vec{\nabla}_{0m} \delta \vec{x}_m &= \vec{\nabla}_{0m} \cdot (\mathbf{P}_m^T \cdot \delta \vec{x}_m) - (\vec{\nabla}_{0m} \cdot \mathbf{P}_m^T) \cdot \delta \vec{x}_m \\ &= \vec{\nabla}_{0m} \cdot (\mathbf{P}_m^T \cdot \delta \vec{x}_m) \end{aligned}$$

and applying the divergence theorem, the volume average of the microstructural virtual work may be expressed in terms

of RVE surface quantities as

$$\frac{1}{V_{0m}} \int_{V_{0m}} \mathbf{P}_m : \delta \mathbf{F}_m^T dV_{0m} = \frac{1}{V_{0m}} \int_{\Gamma_{0m}} \vec{p}_m \cdot \delta \vec{x}_m d\Gamma_{0m} \quad (23)$$

where $\vec{p}_m = \vec{N}_m \cdot \mathbf{P}_m^T$ is the first Piola–Kirchhoff stress vector.

Substitution of the variation of expression (7) into the averaged microwork (23) gives

$$\begin{aligned} &\frac{1}{V_{0m}} \int_{\Gamma_{0m}} \vec{p}_m \cdot (\delta \mathbf{F}_M \cdot \vec{X}_m + \delta \vec{w}_m) d\Gamma_{0m} \\ &= \left(\frac{1}{V_{0m}} \int_{\Gamma_{0m}} \vec{p}_m \otimes \vec{X}_m d\Gamma_{0m} \right) : \delta \mathbf{F}_M^T \\ &\quad + \frac{1}{V_{0m}} \int_{\Gamma_{0m}} \vec{p}_m \cdot \delta \vec{w}_m d\Gamma_{0m} \end{aligned} \quad (24)$$

For the constraints on the microfluctuation field considered in the previous section, that is, the Taylor constraint (13), the uniform displacement boundary conditions (15), and the periodic boundary conditions (17), the last integral involving the RVE average work by the microfluctuation can be shown to vanish from equation (24). Then, comparing equation (24) to the right-hand side of equation (22) allows identification of the macroscopic stress tensor \mathbf{P}_M as

$$\mathbf{P}_M = \frac{1}{V_{0m}} \int_{\Gamma_{0m}} \vec{p}_m \otimes \vec{X}_m d\Gamma_{0m} \quad (25)$$

The above surface integral can further be transformed into a volume integral as follows:

$$\begin{aligned} \mathbf{P}_M &= \frac{1}{V_{0m}} \int_{\Gamma_{0m}} \vec{p}_m \otimes \vec{X}_m d\Gamma_{0m} \\ &= \frac{1}{V_{0m}} \int_{\Gamma_{0m}} \vec{N}_m \cdot \mathbf{P}_m^T \otimes \vec{X}_m d\Gamma_{0m} \\ &= \frac{1}{V_{0m}} \int_{V_{0m}} \vec{\nabla}_{0m} \cdot (\mathbf{P}_m^T \otimes \vec{X}_m) dV_{0m} \\ &= \frac{1}{V_{0m}} \int_{V_{0m}} \mathbf{P}_m dV_{0m} \end{aligned} \quad (26)$$

where first the divergence theorem has been applied and, to obtain the last equality, the following identity, while accounting for the microstructural equilibrium (9) and $\vec{\nabla}_{0m} \vec{X}_m = \mathbf{I}$ (with \mathbf{I} the second-order unit tensor), has been used:

$$\vec{\nabla}_{0m} \cdot (\mathbf{P}_m^T \otimes \vec{X}_m) = (\vec{\nabla}_{0m} \cdot \mathbf{P}_m^T) \otimes \vec{X}_m + \mathbf{P}_m \cdot (\vec{\nabla}_{0m} \vec{X}_m) = \mathbf{P}_m \quad (27)$$

Thus, based on the Hill–Mandel energy consistency relation, for the considered boundary conditions, the macroscale first Piola–Kirchhoff stress tensor has been identified as the volume average of the microscale first Piola–Kirchhoff stress tensor

$$\mathbf{P}_M = \frac{1}{V_{0m}} \int_{V_{0m}} \mathbf{P}_m \, dV_{0m} \quad (28)$$

Note that sometimes in the CH, the stress volume averaging relation (28) is postulated, together with the kinematics scale transition (11), leading to a selection of the boundary conditions, and then the validity of the Hill–Mandel condition is verified. Obviously, the formulations obtained in either way are the same.

4.5 Implementation aspects

4.5.1 RVE boundary value problem

The RVE problem to be solved is a standard nonlinear quasi-static boundary value problem with kinematic boundary conditions.¹ Thus, any numerical technique suitable for solution of this type of problems can be used. In the following, the finite element method will be adopted. Following standard finite element procedures, the weak form of the RVE equilibrium (9) with account for the constitutive relations (10) leads to a system of nonlinear algebraic equations for the unknown nodal displacements \underline{u}

$$\underline{f}_{\text{int}}(\underline{u}) = \underline{f}_{\text{ext}} \quad (29)$$

expressing the balance of internal and external nodal forces. This system has to be completed by boundary conditions. Hence, the earlier introduced boundary conditions (16) or (18) have to be elaborated in more detail.

Fully prescribed boundary displacements

In the case of the fully prescribed displacement boundary conditions (16), the displacements of all nodes on the boundary are simply given by

$$\bar{\underline{u}}_p = (\mathbf{F}_M - \mathbf{I}) \cdot \bar{\underline{X}}_p, \quad p = 1, \dots, N_p \quad (30)$$

where N_p is the number of prescribed nodes, which in this case equals the number of boundary nodes. The boundary conditions (30) are added to the system (29) in a standard manner by static condensation, Lagrange multipliers, or penalty functions.

Periodic boundary conditions

Before application of periodic boundary conditions (18), the equations have to be rewritten into a format more suitable for the finite element framework. Consider the two-dimensional periodic RVE schematically depicted in Figure 2 as an example; extension to three dimensions is straightforward. The boundary of this RVE can be split into four parts, here denoted as “T” top, “B” bottom, “R” right, and “L” left. Taking into account the initial periodicity of the RVE, condition (18) can be rewritten as

$$\begin{aligned} \bar{\underline{u}}_T - \bar{\underline{u}}_B &= (\mathbf{F}_M - \mathbf{I}) \cdot (\bar{\underline{X}}_4 - \bar{\underline{X}}_1) \\ \bar{\underline{u}}_R - \bar{\underline{u}}_L &= (\mathbf{F}_M - \mathbf{I}) \cdot (\bar{\underline{X}}_2 - \bar{\underline{X}}_1) \end{aligned} \quad (31)$$

where $\bar{\underline{X}}_p$, $p = 1, 2, 4$ are the position vectors of the corner nodes 1, 2, and 4 in the undeformed state, see Figure 2.

Prescribing the displacements of the corner nodes in (31) according to

$$\bar{\underline{u}}_p = (\mathbf{F}_M - \mathbf{I}) \cdot \bar{\underline{X}}_p, \quad p = 1, 2, 4 \quad (32)$$

the periodic boundary conditions can be rewritten as

$$\begin{aligned} \bar{\underline{u}}_T &= \bar{\underline{u}}_B + \bar{\underline{u}}_4 - \bar{\underline{u}}_1 \\ \bar{\underline{u}}_R &= \bar{\underline{u}}_L + \bar{\underline{u}}_2 - \bar{\underline{u}}_1 \end{aligned} \quad (33)$$

which is a convenient form for implementation in finite element codes. In a discretized format, the relations (33) lead to a set of homogeneous constraints of the type

$$\underline{C}_a \underline{u}_a = \underline{0} \quad (34)$$

with \underline{C}_a a matrix containing coefficients in the constraint relations and \underline{u}_a a column with the degrees of freedom involved in the constraints. Standard procedures for imposing constraint relations, for example, the direct elimination of the dependent degrees of freedom from the system of equations or the use of Lagrange multipliers or penalty functions, can be applied to impose (34).

4.5.2 Calculation of the macroscopic stress

After the solution of the microstructural RVE boundary value problem, the RVE averaged stress has to be extracted. The macroscopic stress tensor can be calculated by numerically evaluating the volume integral (28). However, it is computationally more efficient to compute the surface integral (25).

Fully prescribed boundary displacements

For the case of prescribed displacement boundary conditions, the surface integral (25) simply leads to

$$\mathbf{P}_M = \frac{1}{V_{0m}} \sum_{p=1}^{N_p} \vec{f}_p \otimes \vec{X}_p \quad (35)$$

where \vec{f}_p are the resulting reaction forces at the boundary nodes and \vec{X}_p the position vectors of these nodes in the undeformed state.

Periodic boundary conditions

For the case of the periodic boundary conditions, the surface integral (25) can be simplified even further. Taking into account that the homogeneous constraints (34) satisfy the condition of zero work, it can be easily shown that the “tying” forces needed to enforce the constraints are antiperiodic and that their contributions to the overall stress tensor cancel out. Thus, for the 2D case considered above, \mathbf{P}_M can be simply computed as

$$\mathbf{P}_M = \frac{1}{V_{0m}} \sum_{p=1,2,4} \vec{f}_p \otimes \vec{X}_p \quad (36)$$

where \vec{f}_p are the resulting reaction forces at the three prescribed nodes.

4.5.3 Macroscopic tangent stiffness

For the solution of nonlinear macroscopic problem using iterative techniques (e.g., Newton–Raphson method), the tangent stiffness is typically required. Since the CH does not provide an explicit form of the macroscopic constitutive relation, the tangent stiffness has to be determined numerically from the relation between variations of the macroscopic stress and macroscopic deformation at every macroscopic (integration) point. This may be realized by numerical differentiation of the numerical macroscopic stress–strain relation, for example, using a forward difference approximation (Miehe, 1996). An alternative approach is the condensation of the microstructural tangent stiffness, used for the solution of the respective RVE problem, to the local macroscopic tangent stiffness. Elaboration of such a procedure in combination with the Lagrange multiplier method to impose boundary constraints can be found in the literature (Miehe, 2002). Here, another scheme (Kouznetsova *et al.*, 2001), which employs the direct condensation of the constrained degrees of freedom, will be outlined.

First, the total microstructural system of equations (in its linearized form) is partitioned as

$$\begin{bmatrix} \underline{K}_{pp} & \underline{K}_{pf} \\ \underline{K}_{fp} & \underline{K}_{ff} \end{bmatrix} \begin{bmatrix} \delta u_p \\ \delta u_f \end{bmatrix} = \begin{bmatrix} \delta f_{\sim p} \\ 0 \end{bmatrix} \quad (37)$$

where δu_p and $\delta f_{\sim p}$ are the columns with iterative displacements and external forces of the prescribed nodes, that is, $p = 1, \dots, N_p$ for prescribed displacement boundary conditions and $p = 1, 2, 4$ for the periodic boundary conditions in 2D; δu_f the column with the iterative displacements of the remaining nodes; and \underline{K}_{pp} , \underline{K}_{pf} , \underline{K}_{fp} , and \underline{K}_{ff} the corresponding partitions of the total RVE tangent stiffness matrix taken at the end of a microstructural increment, when a converged state is achieved. Note that for the case of the periodic boundary conditions, the system (37) should be taken after application of the constraint relations (34). Elimination of δu_f from (37) leads to the reduced stiffness matrix \underline{K}_M relating boundary displacement variations to boundary force variations

$$\underline{K}_M \delta u_p = \delta f_{\sim p}, \quad \text{with} \quad \underline{K}_M = \underline{K}_{pp} - \underline{K}_{pf} (\underline{K}_{ff})^{-1} \underline{K}_{fp} \quad (38)$$

Note that in practice, no direct computation of the inverse $(\underline{K}_{ff})^{-1}$ is needed; instead, if a direct solver is used for the solution of the RVE discrete linear system of equations, the multiplications in the last term of (38) can be performed using the already factorized matrix, thus making the computation of \underline{K}_M rather efficient. For iterative solvers, one can use the procedure developed in Mosby and Matouš (2015a).

Next, the relation between displacement and force variations (38) needs to be transformed to arrive at an expression relating variations of the macroscopic stress and deformation tensors

$$\delta \mathbf{P}_M = {}^4\mathbf{C}_M^P : \delta \mathbf{F}_M^T \quad (39)$$

where the fourth-order tensor ${}^4\mathbf{C}_M^P$ represents the required constitutive tangent stiffness at the macroscopic integration point level.

To obtain this constitutive tangent from the reduced stiffness matrix \underline{K}_M , it is convenient to first rewrite the relation (38) in a specific vector/tensor format

$$\sum_j \mathbf{K}_M^{(ij)} \cdot \delta \vec{u}_{(j)} = \delta \vec{f}_{(i)} \quad (40)$$

where indices i and j take the values $i, j = 1, \dots, N_p$ for prescribed displacement boundary conditions and $i, j = 1, 2, 4$ for the periodic boundary conditions. In (40), the components of the tensors $\mathbf{K}_M^{(ij)}$ are simply found in the tangent matrix \underline{K}_M at the rows and columns of the degrees of freedom in the nodes i and j . Next, the expression for

the variation of the nodal forces (40) is substituted into the relation for the variation of the macroscopic stress following from (35) or (36)

$$\delta \mathbf{P}_M = \frac{1}{V_{0m}} \sum_i \sum_j (\mathbf{K}_M^{(ij)} \cdot \delta \vec{u}_{(j)}) \otimes \vec{X}_{(i)} \quad (41)$$

Substitution of the relation for the prescribed nodes $\delta \vec{u}_{(j)} = \vec{X}_{(j)} \cdot \delta \mathbf{F}_M^T$ into (41) gives

$$\delta \mathbf{P}_M = \frac{1}{V_{0m}} \sum_i \sum_j (\vec{X}_{(i)} \otimes \mathbf{K}_M^{(ij)} \otimes \vec{X}_{(j)})^{LT} : \delta \mathbf{F}_M^T \quad (42)$$

where the superscript LT denotes transposition on the two left indices. Finally, by comparing (42) with (39), the consistent constitutive tangent is identified as

$${}^4 C_M^P = \frac{1}{V_{0m}} \sum_i \sum_j (\vec{X}_{(i)} \otimes \mathbf{K}_M^{(ij)} \otimes \vec{X}_{(j)})^{LT} \quad (43)$$

4.6 Computational homogenization for multiphysics problems

As described in Section 3.4, the CH framework has been extended to various multiphysics problems. In many cases, extensions and applications to coupled fields can be done largely along the same lines as described above for purely mechanical problems. In this case, the unknown displacement (position vector) field is replaced by another field, for example, temperature, electric potential, magnetic potential, and so on, see, for example, Özdemir *et al.* (2008a,b), Schröder and Keip (2012), Zäh and Miehe (2013), Javili *et al.* (2013) for more details. The multiscale procedure is then driven by the gradient of this field, for example, temperature gradient, electric field, and magnetic field. Postulating a scale transition relation for this gradient quantity, similar to equation (11), yields the condition on the microfluctuation field that is used to formulate the RVE boundary conditions on the unknown field. The Hill–Mandel macrohomogeneity condition (22) is generalized in terms of the product of the gradient field and its dual, for example, temperature gradient and heat flux, electric field and electric displacement, and magnetic field and magnetic induction, from which the expression for the homogenized dual quantity is derived, usually in the form of both volume and surface integrals. At each scale, appropriate balance equations are solved. Due to the scale separation requirement, the RVE problem has to be stationary, while the macroscopic problem can be transient. The derivation of the macroscopic tangent operator for nonlinear iterations can be performed in a similar way through static condensation, as described above.

Additional difficulty appears in some problems due to the need to prescribe not only the gradient quantity on the RVE, for example, the temperature gradient, but also the absolute level of the unknown field quantity, for example, the temperature itself in case of the temperature-dependent material properties. In this case, additional scale transition relations need to be formulated. For example, in Özdemir *et al.* (2008a,b), the thermal energy consistency condition was enforced by requiring the volume average of the RVE stored heat to be equal to the local macroscopic stored heat. After elaboration, this has led to an additional constraint on the RVE temperature field.

5 RVE ASPECTS AND STATISTICS FOR NONLINEAR MATERIALS

As alluded to in the previous sections, the RVE used in the context of CH has various definitions. The definition proposed by Hill (1963) implies that the RVE should be large enough to represent a whole ensemble of microstructures in an average sense, and contain a sufficient number of heterogeneities in order to eliminate boundary effects, as long as the boundary values are macroscopically uniform. Drugan and Willis (1996) proposed a variant, where the RVE is the smallest material volume element that represents the mean constitutive response with sufficient accuracy. Povirk (1995) proposed yet another approach to determine the RVE that relies on a description of the microstructure using a certain statistical descriptor function. An optimally sized domain that preserves the statistical description of the original microstructure is regarded as the RUC. In all these cases, an RVE should be both statistically representative (i.e., capture geometrical complexity of a material) and should capture the effective material behavior (i.e., capture physical response of a material). We focus on randomly configured microstructures in this section and show that both requirements are mutually inclusive, since properly capturing the morphology leads to sufficiently accurate overall behavior. In summary, an ideal RVE for random morphologies is only achievable in the infinite volume limit, but an optimally constructed RUC can lead to effective material predictions with small deviation.

5.1 Image-based modeling

When modeling geometric and material nonlinearities in heterogeneous materials, construction of an appropriate computational microscale domain or RUC for multiscale

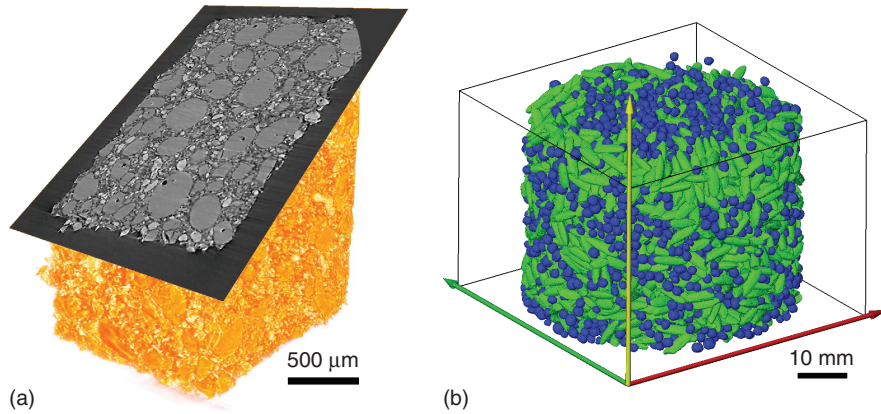


Figure 3. Three-dimensional representations of microstructures obtained using micro-CT. (a) Solid rocket propellant (from Lee *et al.*, 2011). (b) Granular pack of polydisperse spheres (black mustard) and ellipsoids (rice grains) (from Gillman *et al.*, 2013).

simulations is crucial for obtaining accurate predictions. Moreover, analyzing realistic microstructures is critical for simulations to become truly predictive.

The concept of image-based (data-driven) modeling focuses on obtaining detailed three-dimensional data sets from imaging methods, for example, microcomputer tomography (micro-CT) or scanning electron microscopy (SEM), and constructing optimal computational domains. Micro-CT is a particularly attractive imaging method, as it allows for three-dimensional representations to be obtained nondestructively. Some examples of complex material systems imaged with micro-CT are shown in Figure 3. Note that heterogeneous materials may contain a variety of heterogeneous phases (voids, inclusions, fibers, crystals, etc.) of varying composition, size, and shape with complex spatial configuration, and statistically preserving this morphology in an RUC is critical.

5.2 Statistically representative unit cells

The random complex nature of heterogeneous microstructures makes volume-averaged statistical descriptors well suited for quantifying the spatial configuration.

5.2.1 Statistical descriptors

Many statistical descriptors of heterogeneous materials have been proposed to quantify random morphologies, see the book by Torquato (2002), for example. One common measure is the n -point probability function. First, an indicator function of material phase q at a position $\vec{x} \in \mathbb{R}$ is given by

$$\chi_q(\vec{x}) = \begin{cases} 1 & \text{if } \vec{x} \text{ in phase } q \\ 0 & \text{otherwise.} \end{cases} \quad (44)$$

The n -point probability function is then defined as the ensemble average (denoted by an overbar) of the indicator function for n points as

$$S_{qs\dots t}(\vec{x}_1, \vec{x}_2, \dots, \vec{x}_n) = \overline{\chi_q(\vec{x}_1)\chi_s(\vec{x}_2)\cdots\chi_t(\vec{x}_n)} \quad (45)$$

which represents the probability of phases q, s, \dots, t existing at points $\vec{x}_1, \vec{x}_2, \dots, \vec{x}_n$, simultaneously.

In what follows, we will focus on statistically homogeneous (translationally invariant) and isotropic (rotationally invariant) microstructures for ease of presentation. Generalization to more complex anisotropic systems can be found in Torquato (2002) and Gillman *et al.* (2013). For ergodic, homogeneous, and isotropic systems, the one- and two-point probability functions reduce to $S_q(\vec{x}_1) = c_q$, $S_{qs}(\vec{x}_1, \vec{x}_2) = S_{qs}(r = |\vec{x}_2 - \vec{x}_1|)$, where c_q is the volume fraction of constituent q (Figure 4a). Moreover, randomly configured microstructures lack long-range order, and the following limits hold for the two-point probability functions

$$S_{qs}(\vec{x}_2 - \vec{x}_1) \rightarrow \begin{cases} c_q \delta_{qs} & \text{as } \vec{x}_2 - \vec{x}_1 \rightarrow \vec{0} \\ c_q c_s & \text{as } \vec{x}_2 - \vec{x}_1 \rightarrow \vec{\infty} \end{cases} \quad (46)$$

The limit case $\vec{x}_2 - \vec{x}_1 \rightarrow \vec{\infty}$ is a natural candidate for determining a minimum geometric size of an RUC and is discussed below.

Analytical expressions of the n -point probability functions typically cannot be defined for random morphologies. Therefore, Monte Carlo-based statistical sampling algorithms are often utilized, where many random samples are considered. An adaptive sampling strategy for up to third-order statistics is presented in Gillman and Matouš (2014). An example of the isotropic two-point probability function, S_{pp} , is shown in Figure 4(b).

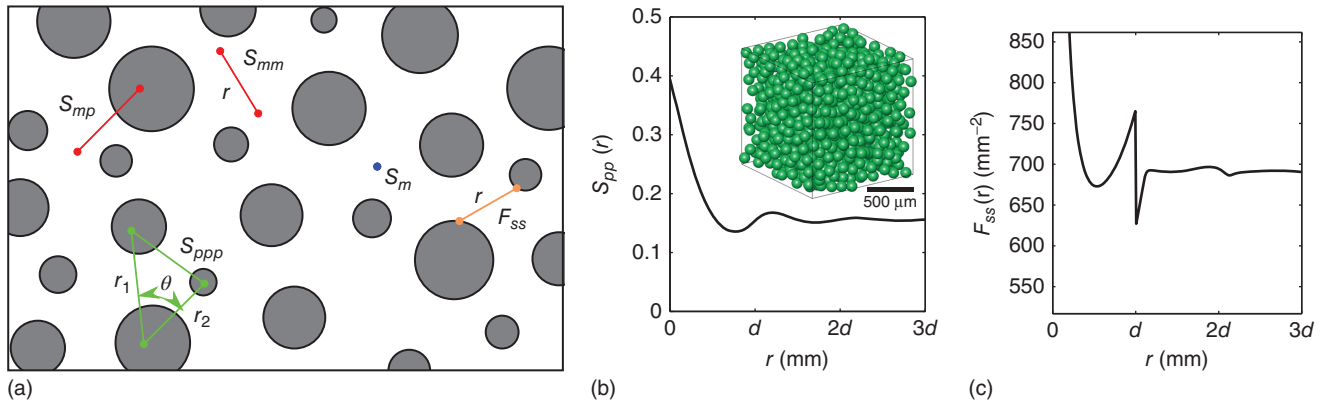


Figure 4. (a) Illustration of the n -point probability and surface–surface correlation functions. (b) Two-point probability. (c) Surface–surface correlation function for a microstructure with 1000 spheres of diameter $d = 91.4 \mu\text{m}$ and $c_p = 0.4$ (see inset of (b)). Note that the subscripts p , m , and s denote the particulate, matrix, and interphase constituents, respectively.

Although n -point probability functions have frequently been used for quantifying random microstructures, some microscale models may require additional statistical descriptors. For instance, when considering imperfect surface phenomena, such as particle–matrix debonding or nanoscale interphases, surface–surface correlation functions may be relevant descriptors for analysis. The surface–surface correlation function can be defined in the limit of an interphase of thickness t going to zero as

$$F_{ss}(r) = \lim_{t \rightarrow 0} \frac{S_{ss}(r)}{t^2} \quad (47)$$

where S_{ss} is the two-point probability function of the interphase s . This function is presented for a pack of spheres with $t = 0.01d$ in Figure 4(c). Moreover, note that other statistical descriptors, for example, radial distribution (pair correlation), lineal path, and chord length density functions, have been used to characterize heterogeneous materials (Yeong and Torquato, 1998; Bochenek and Pyrz, 2004; Zeman and Šejnoha, 2007). The choice of these statistical measures depends on the material system and physics of interest.

Note that these statistical descriptors are not solely utilized for quantifying the morphology, but also arise in micromechanics estimates of effective thermomechanical behavior for both linear (Torquato, 2002; Milton, 2002; Lee *et al.*, 2011; Gillman *et al.*, 2013, 2015) and nonlinear (Talbot and Willis, 1985; Ponte Castañeda, 1998) regimes. In an article by Gillman *et al.* (2015), third-order statistical micromechanics models showed that the effective thermomechanical properties for packs of platonic solids are altered substantially by changing the particle shape.

5.2.2 RUC reconstruction

In order to construct an optimal RUC that preserves the statistical makeup of large composite microstructures, an optimization problem is typically formulated. In this section, we discuss reconstructing RUCs of the second order (i.e., first- and second-order statistics are preserved). A general objective function, f , which quantifies the differences in relevant statistical descriptors, S_i , between a large image-based data set (denoted by superscript p) and an RUC (denoted by superscript c) is defined as

$$f(\vec{\mathcal{X}}) = \sum_i^{N_i} \alpha_i \mathcal{F}_i + \sum_i^{N_p} \beta_i \mathcal{P}_i, \mathcal{F}_i = |S_i^p - S_i^c| \quad (48)$$

where $\vec{\mathcal{X}}$ is the set of physically admissible geometric parameters subject to minimization. Here, \mathcal{P}_i are penalty functions to enforce geometric constraints such as impenetrability, N_s and N_p are the number of statistics functions and number of penalty functions, respectively, and α_i and β_i are weights for each term in the objective function.

When considering n -point probability functions of heterogeneous materials, two separate objective functions can be minimized independently. A first objective function is formulated to determine the geometrical size of the cell, l_{cell} , that best preserves volume fractions (first-order statistics) given the number and volume of constituents. This objective function for an N -phase material is defined as

$$F_1(l_{\text{cell}}) = \sqrt{\sum_q^N (c_q^p - c_q^c)^2} = \sqrt{\sum_q^N \left(c_q^p - \frac{V_q n_q}{l_{\text{cell}}^3} \right)^2} \quad (49)$$

where c_q^p and c_q^c are the volume fractions for material phase q . V_q and n_q are the volume and the number of heterogeneous phases (i.e., geometric entities—particles, fibers, voids) in the cell for phase q . The saturation point of the two-point probability function (r_{sat}), which is the point at which derivatives of all two-point probability functions reach zero (46), provides a good initial guess, $l_{\text{stat}} = 2r_{\text{sat}}$, for optimal l_{cell} . Thus, l_{stat} is the smallest sample that can statistically describe the overall material morphology up to the second-order probability functions. A second objective function minimizing the L_2 error of the isotropic two-point statistics is defined as

$$\mathcal{F}_2(\vec{x}_n) = \sum_q \sum_s^N \|S_{qs}^p - S_{qs}^c\|_{L_2} \quad (50)$$

where \vec{x}_n are the positions of the geometric features in the microscale cell. Anisotropic materials or statistics of the higher order can be described in a similar way but are not covered for brevity of presentation.

An example of this reconstruction procedure is presented here from Lee *et al.* (2009), where particulate RUCs are reconstructed from a tomographically obtained data set for a granular system of polydisperse silica (see inset of Figure 5a). A large section (pack, see Figure 5b) from the tomographic data set ($1445.37 \times 1287.892 \times 789.106 \mu\text{m}^3$) containing 19 892 particles is analyzed. The particles are grouped into nine different sizes/modes (Figure 5a), and two-point probability functions are computed. From the statistical analysis of the pack, the statistical length scale is $l_{\text{stat}} = 2r_{\text{sat}} = 400 \mu\text{m}$ (~ 10 mean particle diameters). Utilizing this statistical information, five RUCs of the second statistical order were reconstructed using a genetic algorithm. Each RUC contains 1082 particles with $l_{\text{cell}} = 399.632 \mu\text{m}$ (geometric length scale), and one of

these cells is shown in Figure 5(b). Adequate agreement in the two-point statistics is illustrated in Figure 5(c). Note the small standard deviation over five cell realization indicating a small error in cell morphologies. It is important to note that the particle packing density and particle size distribution play a critical role in the resulting statistical/geometric length scale, that is, highly filled systems result in larger l_{cell} (Collins *et al.*, 2010).

5.3 Numerical example: failure in heterogeneous interfaces

Utilizing the statistical reconstruction framework summarized in Section 5.2.2, we illustrate the connection between the geometric material length scale, $l_{\text{cell}} \approx l_{\text{stat}}$, and the physical size of an RUC, l_{RUC} , that is required to describe the effective nonlinear material behavior. As mentioned at the beginning of this section, the morphology/geometry of an RUC and its effective material behavior are closely intertwined. In particular, the failure response of three different-sized cells is computed in the context of multiscale cohesive modeling in a 3D finite strain setting (Matouš *et al.*, 2008; Kulkarni *et al.*, 2009, 2010; Mosby and Matouš, 2015a,b). Microscale failure is modeled with a viscous isotropic damage model (Simo and Ju, 1989; Matouš *et al.*, 2008). Five statistically (macroscopically) equivalent RUCs of different morphology (microstructure) for each cell size were considered, and the averaged normal traction–separation curves were computed. The traction–separation response is shown in Figure 6(a) with error bars showing one standard deviation over five cell realizations. Here, p_M^n and $[[u_M^n]]$ are the normal macroscopic traction and jump in displacement at the interface, respectively. When comparing the averaged response, the

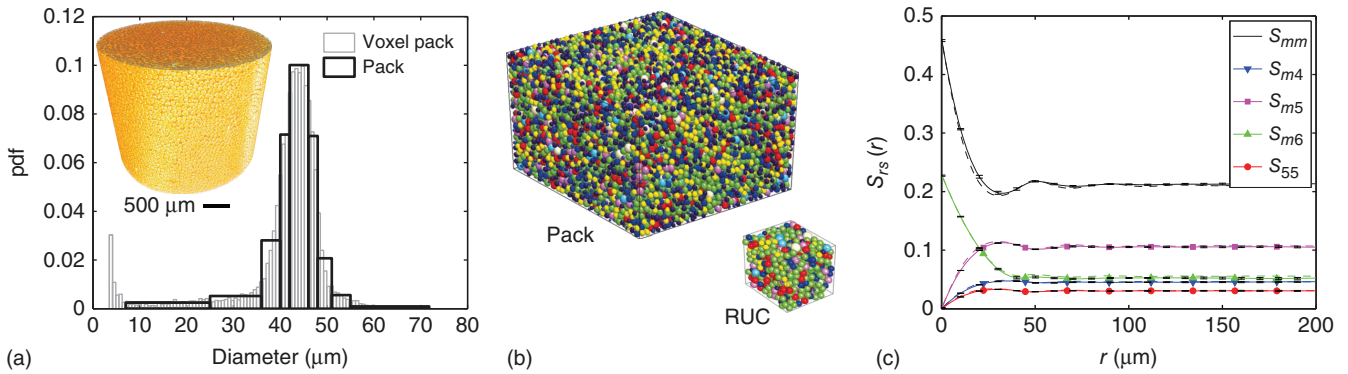


Figure 5. RVE reconstruction example (from Lee *et al.*, 2009) based on minimizing differences in one- and two-point probability functions for a granular pack of silica. (a) Particle size distribution from tomographically obtained characterization (see inset image). (b) Pack and a reconstructed RUC. (c) Comparison of two-point probability functions between the pack (dashed lines) and mean/standard deviations of five reconstructed RUCs (solid lines).

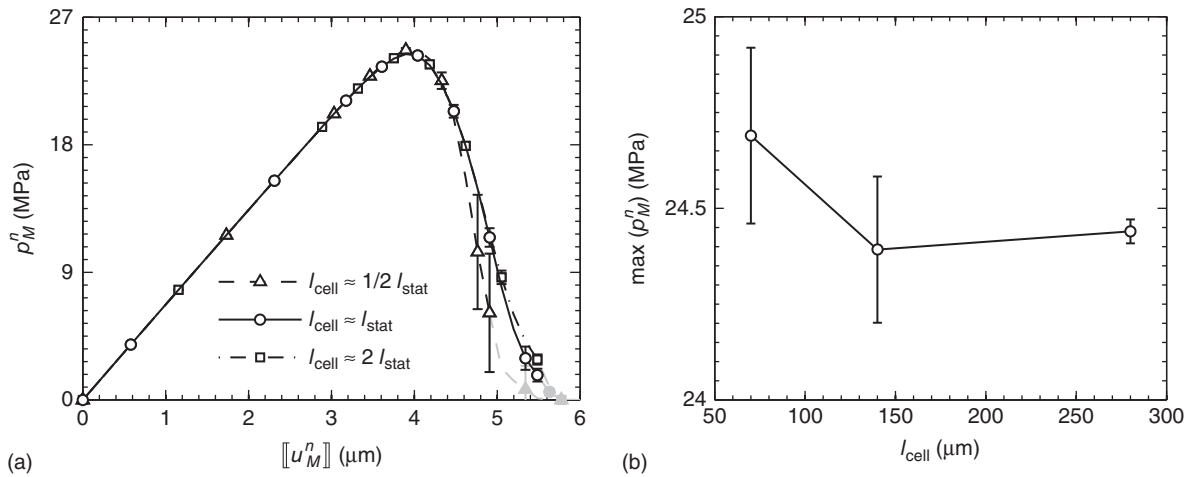


Figure 6. Effect of cell size on macroscopic traction–separation response (from Mosby and Matouš, 2015b). Note that the statistical length scale for this material is $l_{\text{stat}} = 140 \mu\text{m}$. (a) Comparison of the average normal traction–separation response for different-sized cells. (b) Convergence of the normal strength with increasing cell size.

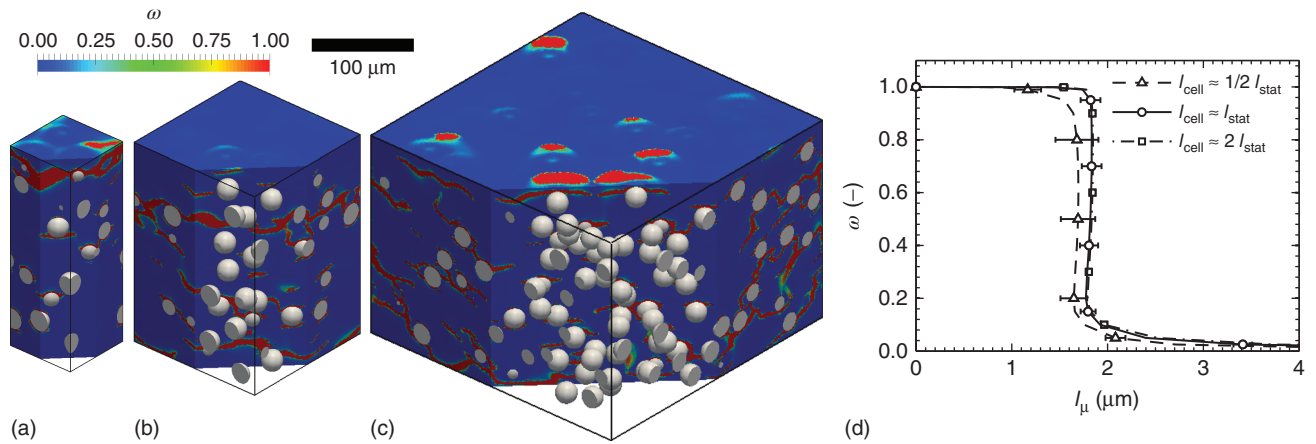


Figure 7. Comparison of the damage pattern at the final computed point in cells with different side lengths (from Mosby and Matouš, 2015b). (a–c) Visualization of different-sized cells. (d) Effective crack thickness at the last computed point. The effective crack thickness is defined as $l_\mu = V|_\omega / A|_\omega$, where $V|_\omega$ is the volume of material damaged beyond a threshold value of the damage variable and ω , and $A|_\omega$ the one half of the corresponding surface area of the damaged volume.

hyperelastic behavior is identical for all cell sizes, but the limit point and softening responses are not. This illustrates the key effect of nonlinearity on the resulting size of the RUC. While the two larger unit cells ($l_{\text{cell}} \approx l_{\text{stat}}$ and $l_{\text{cell}} \approx 2l_{\text{stat}}$) have small and overlapping error bars, the smallest cell ($l_{\text{cell}} \approx 1/2l_{\text{stat}}$) has a distinctly different softening response with large standard deviation. One important quantity of interest is the maximum traction (strength). The convergence of the normal strength with respect to the side length of the unit cell, l_{cell} , is displayed in Figure 6(b). This figure shows the rapid convergence of both mean and standard deviation with increasing cell size.

The damage pattern at the final computed points (last open black symbols in Figure 6(a)) is also analyzed in Figure 7(a–c). Notice that the two larger cells have a more distributed damage pattern, whereas the cell with $l_{\text{cell}} \approx 1/2 l_{\text{stat}}$ has a single dominant crack at the top of the cell. In this example, the microstructural length scale of interest is the effective crack thickness denoted as l_μ (5). The effective crack thickness for different threshold values of the damage variable, ω , is shown in Figure 7(d). As shown, l_μ is nearly identical for the two larger cells, while the smallest cell has a smaller effective crack thickness.

For this example, it is clear that cells smaller than the statistical length scale ($l_{\text{cell}} < l_{\text{stat}}$) are incapable of predicting the highly nonlinear effective material response. Cells with $l_{\text{cell}} \geq l_{\text{stat}}$ provide a more accurate and precise material description, yet they are computationally expensive. Therefore, the required accuracy of the overall macroscopic response needs to be balanced with the resulting increase in computational cost. Finally, note once more that the relationship between the RUC size (l_{RUC}) and l_{cell} is not solely dependent on the microstructure, as the constituent material properties and their contrast also play a role. Therefore, the RUC size analysis summarized here (both based on morphology, Section 5.2, and physics, Section 5.3) should be completed for any given material system of interest before concluding that $l_{\text{RUC}} = l_{\text{cell}} \approx l_{\text{stat}}$. Nevertheless, the statistical characteristic length scale is a good candidate for RUC construction.

6 DECOUPLED COMPUTATIONAL HOMOGENIZATION METHODS

To circumvent computational cost issues related to nested calculations in CH methods, as described in Section 4, alternative approaches have been introduced with the aim of developing *decoupled* numerical methods for homogenizing heterogeneous materials with nonlinear or time-dependent behaviors. A first straightforward approach, inspired by classical experimental identifications procedures, uses virtual tests on RVEs through numerical computations to identify empirical macroscopic constitutive laws (see, e.g., recent contributions in Terada *et al.*, 2013, 2014). However, classifying such procedures as homogenization is questionable. Constructing effective constitutive laws without prior knowledge on their form is, however, possible, but in some restricted cases. A second class of techniques is based on the construction of a numerical, material map between effective stress and strains (Terada and Kikuchi, 1995; Takano *et al.*, 1996; Temizer and Wriggers, 2007; Yvonnet *et al.*, 2009, 2013; Clément *et al.*, 2012; Tran *et al.*, 2011), which can be applied, for example, in the case of hyperelastic materials or for linear viscoelasticity, as described in the following. A third class of methodologies, valid for viscoplastic materials at small strains, uses preliminary computations to construct a basis for anelastic modes (TFA and NTFA techniques). We describe these techniques in Section 6.3.

6.1 Decoupled approach for nonlinear elasticity at finite strains

A consequence of the Hill–Mandel lemma discussed in Section 4, see equation (22), is that the macroscopic first

Piola–Kirchhoff stress tensor can be defined according to:

$$\mathbf{P}_M = \langle \mathbf{P}_m \rangle = \frac{\partial \Psi_M^*(\mathbf{F}_M)}{\partial \mathbf{F}_M} \quad (51)$$

where $\langle \cdot \rangle$ denotes spatial averaging over the domain associated with the RVE in the reference configuration and $\Psi_M^*(\mathbf{F}_M)$ defines the strain energy density function or elastic potential associated with the homogeneous equivalent material, determined by

$$\begin{aligned} \Psi_M^*(\mathbf{F}_M) &= \inf_{\mathbf{F}_m \in \mathcal{K}^*(\mathbf{F}_M)} \langle \Psi_m^*(\vec{\mathbf{X}}, \mathbf{F}_m) \rangle \\ &= \inf_{\mathbf{F}_m \in \mathcal{K}^*(\mathbf{F}_M)} \sum_{r=1}^N c_r \langle \Psi_m^{*r}(\mathbf{F}_m) \rangle^r \end{aligned} \quad (52)$$

where \mathcal{K}^* is the set of kinematically admissible deformation gradient tensors, N the number of phases, and c_r the volume fractions of the different phases. It can be shown that Ψ_M^* is objective. Thus, $\Psi_M^*(\mathbf{F}_M) = \Psi_M(\mathbf{C}_M)$. It is worth noting that only \mathbf{F}_M and \mathbf{P}_M can be defined as the volume spatial averages of their microscopic counterparts. Furthermore, we have the relations

$$\mathbf{S}_M = \mathbf{F}_M^{-1} \cdot \mathbf{P}_M, \quad \boldsymbol{\sigma}_M = \frac{1}{J_M} \mathbf{P}_M \cdot \mathbf{F}_M^T \quad (53)$$

with $J_M = \langle \det(\mathbf{F}_m) \rangle$. A similar relation to equation (51) can be stated to relate the effective second Piola–Kirchhoff stress \mathbf{S}_M and right Cauchy–Green deformation \mathbf{C}_M . Using (51), we have

$$\mathbf{P}_M = \left(\frac{\partial \mathbf{C}_M}{\partial \mathbf{F}_M} \right) : \frac{\partial \Psi_M(\mathbf{C}_M)}{\partial \mathbf{C}_M} \quad (54)$$

and

$$\left(\frac{\partial \mathbf{C}_M}{\partial \mathbf{F}_M} \right) = 2(\mathbf{F}_M^T \underline{\underline{\mathbf{I}}}) \quad (55)$$

where we note the product $(\mathbf{A} \underline{\underline{\mathbf{B}}})_{ijkl} = \frac{1}{2}(A_{ik}B_{jl} + A_{il}B_{jk})$. Then, we have

$$\mathbf{S}_M = \mathbf{F}_M^{-1} \cdot \mathbf{P}_M = 2(\underline{\underline{\mathbf{I}}}) : \frac{\partial \Psi_M(\mathbf{C}_M)}{\partial \mathbf{C}_M} \quad (56)$$

After simplifications and using the symmetry of \mathbf{C}_M , we obtain

$$\mathbf{S}_M = 2 \frac{\partial \Psi_M(\mathbf{C}_M)}{\partial \mathbf{C}_M} \quad (57)$$

Then, the effective strain-density function Ψ_M of the composite can be defined as

$$\begin{aligned}\Psi_M(\mathbf{C}_M) &= \inf_{\vec{c}_m \in \mathcal{K}(\mathbf{C}_M)} \langle \Psi_m(\vec{X}, \mathbf{C}_m) \rangle \\ &= \inf_{\vec{c}_m \in \mathcal{K}(\mathbf{C}_M)} \sum_{r=1}^N c_r \langle \Psi_m^r(\mathbf{C}_m) \rangle^r\end{aligned}\quad (58)$$

where \mathcal{K} is the set of kinematically admissible deformation tensors for \mathbf{C}_M . In other words, for a given macroscopic deformation state \mathbf{C}_M , the corresponding value of $\Psi_M(\mathbf{C}_M)$ is found by evaluating the average of local potential functions $\Psi_m(\vec{X}, \mathbf{C}_m)$, where $\mathbf{C}_m(\vec{X})$ is an admissible deformation field. Using similar arguments, the macroscopic elastic tangent tensor ${}^4\mathbb{L}_M$ can be expressed as

$${}^4\mathbb{L}_M = 4 \frac{\partial^2 \Psi_M(\mathbf{C}_M)}{\partial \mathbf{C}_M^2} \quad (59)$$

In the NEXP method (Yvonnet *et al.*, 2009, 2013), the effective behavior of nonlinear materials is obtained by means of a database describing the overall potential $\Psi_M(\mathbf{C}_M)$, which is evaluated and interpolated numerically in the space of macroscopic deformation components as

$$\Psi_M(\mathbf{C}_M) \approx \sum_i N_i(\mathbf{C}_M) \Psi_{Mi} \quad (60)$$

where N_i are interpolation functions in the macroscopic deformation domain. For this purpose, finite element computations are performed on an RVE for each point of the deformation domain, which corresponds to boundary conditions for the local nonlinear problem. Once computed and stored, the discrete values of the potential Ψ_{Mi} can be interpolated and derived for obtaining the stress S_M as

$$S_M(\mathbf{C}_M) \approx 2 \sum_i \frac{\partial N_i(\mathbf{C}_M)}{\partial \mathbf{C}_M} \Psi_{Mi} \quad (61)$$

Finally, the elastic tangent tensor, ${}^4\mathbb{L}_M$ (required at each macroscale integration point to solve the macroscopic boundary value problem), is computed according to

$${}^4\mathbb{L}_M(\mathbf{C}_M) \approx 4 \sum_i \frac{\partial^2 N_i(\mathbf{C}_M)}{\partial \mathbf{C}_M^2} \Psi_{Mi} \quad (62)$$

As the local problem is solved with the purpose of computing the potential $\Psi_M(\mathbf{C}_M)$, it is necessary to define boundary conditions on the RVE with respect to \mathbf{C}_M . Since Ψ_M does not depend on rotations, \mathbf{R}_M , we can choose $\mathbf{R}_M = \mathbf{I}$, which leads to $\mathbf{F}_M = \mathbf{U}_M = \mathbf{C}_M^{1/2}$. Then, the RVE boundary conditions, for example,

periodic, can further be prescribed as was elaborated in Section 4.5 (7) as

$$\Delta \vec{x}_m = \mathbf{C}_M^{1/2} \cdot \Delta \vec{X}_m + \vec{w}_m \quad \text{on} \quad \Gamma_{0M} \quad (63)$$

6.2 Decoupled approach for homogenization of linear viscoelastic composites

Here, we consider a composite whose phases are linear viscoelastic and assume small strains. In that case, it can be shown that the effective or macroscopic behavior of the composite remains linearly viscoelastic (Hashin, 1965, 1970) and is generally characterized by

$$\begin{aligned}\sigma_M(t) &= \int_{-\infty}^t {}^4\mathbb{T}_M(t-s) : \frac{d\epsilon_M(s)}{ds} ds \\ &= \int_0^t {}^4\mathbb{T}_M(t-s) : \frac{d\epsilon_M(s)}{ds} ds + {}^4\mathbb{T}_M(t) : \epsilon_M(0)\end{aligned}\quad (64)$$

where $\sigma_M(t) = \langle \sigma_m(t) \rangle$ and $\epsilon_M(t) = \langle \epsilon_m(t) \rangle$. In the general case, that is, for arbitrary RVE morphology and different local viscoelastic models, the form of the effective fourth-order relaxation tensor, ${}^4\mathbb{T}_M$, is unknown. However, a numerical approximation of ${}^4\mathbb{T}_M(t)$ can be constructed, as proposed by Tran *et al.* (2011). For this purpose, the numerically explicit mapping $[{}^4\mathbb{T}]_{ijkl} : \mathbb{R}^+ \rightarrow \mathbb{R}$ is introduced and is defined as

$$[{}^4\mathbb{T}]_{ijkl}(t) \simeq \sum_{p=1}^M \phi_p^{ijkl}(t) \alpha_p^{ijkl} \quad (65)$$

where M is the number of nonzero shape functions at time t , α_p^{ijkl} the components of the effective relaxation tensor function sampled at time t_p such that

$$[{}^4\mathbb{T}]_{ijkl}(t^p) \equiv \alpha_p^{ijkl} \quad (66)$$

and $\phi_p^{ijkl}(t)$ the interpolation function related to the time step t^p . In (64), no sum holds for indices i, j, k , and l . By choosing

$$\epsilon_M(t) = H(t) \epsilon_M^{(ij)} \quad (67)$$

where $H(t)$ is the Heaviside step function and $\epsilon_M^{(ij)}$ an elementary strain state defined below, and by introducing (67) in (64), we obtain

$$\sigma_M(t) = \int_{-\infty}^t {}^4\mathbb{T}_M(t-s) : \epsilon_M^{(ij)} \delta(s) ds \quad (68)$$

with $\delta(t)$ being the Dirac delta function. With the help of the property

$$\int_{-\infty}^t f(t-s)\delta(s)ds = f(t) \quad (69)$$

we finally have

$$[{}^4\mathbb{T}_M(t)]_{ijkl} = \frac{\sigma_{Mij}^{(kl)}(t)}{\bar{\epsilon}_0} = \frac{\langle \sigma_{mij}^{(kl)}(t) \rangle}{\bar{\epsilon}_0} \quad (70)$$

where $\sigma_{mij}^{(kl)}(t)$ is the second-order stress field in the RVE obtained numerically by solving a transient problem for an RVE with linear viscoelastic phases when applying a macroscopic strain in the form

$$\epsilon_M^{(kl)} = \frac{1}{2}\bar{\epsilon}_0(\vec{e}_k \otimes \vec{e}_l + \vec{e}_l \otimes \vec{e}_k), \quad k = 1, \dots, 3, \quad l = 1 \dots 3 \quad (71)$$

In (70) and (71), $\bar{\epsilon}_0$ is an arbitrary constant, small enough to keep the resulting microscopic and macroscopic strains small and ensuring that no geometrical and mechanical nonlinearities occur. Then, a simple algorithm can be defined to compute the response of the FE structure at the macroscopic scale (see Tran *et al.*, 2011 for more details). An illustration of a structural simulation by such technique is provided in Figure 8.

6.3 NTFA method (nonuniform transformation field analysis)

In this approach, the microstructural constituents are assumed to be generalized standard materials (see Halphen and Nguyen, 1975 or Germain, 1983). For all points within the material, the state is defined by the infinitesimal strain

tensor, ϵ_m , and a vector of state internal variables α_m associated with dissipative phenomena such as plasticity or damage. Stress and thermodynamic forces are given by the relationship

$$\sigma_m = \frac{\partial w_m}{\partial \epsilon_m}(\epsilon_m, \alpha_m), \quad \Xi_m = -\frac{\partial w_m}{\partial \alpha_m}(\epsilon_m, \alpha_m) \quad (72)$$

where the free energy w is a convex functions of its arguments. The evolution of internal variables is given by

$$\dot{\alpha}_m = \frac{\partial \psi_m}{\partial \Xi_m}(\Xi_m), \quad \text{or} \quad \Xi_m = \frac{\partial \varphi_m}{\partial \dot{\alpha}_m}(\dot{\alpha}_m) \quad (73)$$

where φ_m and ψ_m are dual, convex potentials. We first describe the TFA method, initially proposed by Dvorak (1992). We consider the following equations of the local problem defined on the RVE, which is associated with an open domain Ω_m containing interfaces collectively denoted by Γ_m :

$$\vec{\nabla} \cdot \sigma_m(\vec{x}) = \vec{0} \quad \text{in } \Omega_m \setminus \Gamma_m \quad (74)$$

$$\langle \epsilon_m(\vec{x}) \rangle = \epsilon_M \quad (75)$$

$$\sigma_m(\vec{x}) = {}^4C_m(\vec{x}) : (\epsilon_m(\vec{x}) - \epsilon_m^{an}(\vec{x})) \quad (76)$$

where ${}^4C_m(\vec{x})$ is the elastic tensor and $\epsilon_m^{an}(\vec{x})$ a tensor of anelastic strains. Introducing (76) in (74) and considering (75), the strain solution of the linear problem (74)–(76) can be formally expressed using the superposition principle as

$$\epsilon_m(\vec{x}) = {}^4A_m(\vec{x}) : \epsilon_M + \int_{\Omega_m} {}^4D_m(\vec{x}, \vec{y}) : \epsilon_m^{an}(\vec{y}) d\Omega_y \quad (77)$$

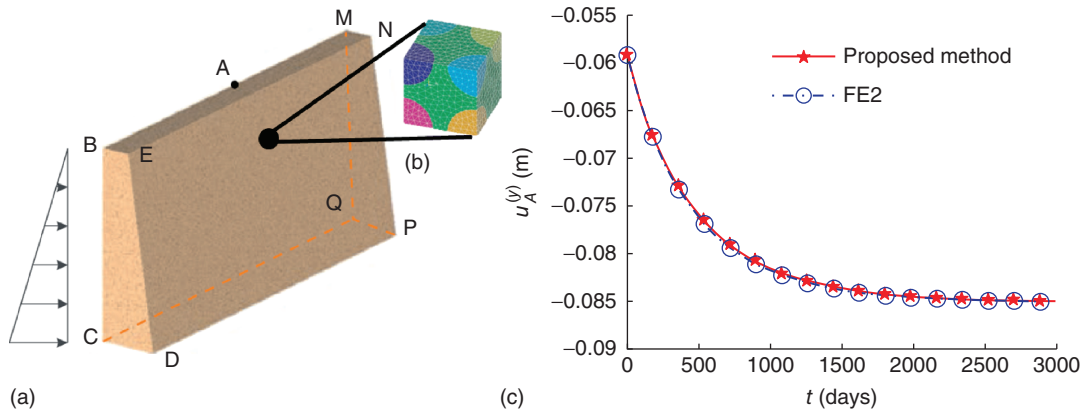


Figure 8. Homogenization of heterogeneous viscoelastic material by decoupled approach (adapted from Tran *et al.* (2011)): (a) structure; (b) RVE; (c) response of the structure to a permanent load in time.

In (77), ${}^4\mathbb{A}_m(\vec{x})$ is the classical localization tensor, ${}^4\mathbb{D}_m$ the fourth-order Green operator defined over Ω_m , and $d\Omega_y$ denotes integration with respect to the \vec{y} variable. In this form, using (76) and taking the spatial average of the stress $\sigma_M = \langle \sigma_m(\vec{x}) \rangle$, we obtain a relationship among the macroscopic stress, the macroscopic strain, and the local (microscopic) anelastic strain field $\epsilon_m^{an}(\vec{x})$, corresponding to an infinite number of internal variables. From now on, for the sake of clarity, new introduced quantities without subscript m will denote microscale quantities.

The idea of the TFA method is to reduce the number of internal variables by expanding $\epsilon_m^{an}(\vec{x})$ as

$$\epsilon_m^{an}(\vec{x}) = \sum_{r=1}^N \epsilon_r^{an} \chi_r(\vec{x}) \quad (78)$$

where $\chi_r(\vec{x})$ is a characteristic indicator function (44) and ϵ_r^{an} is a uniform eigenstrain defined in each phase. Introducing (78) in (74)–(76), $\epsilon_m(\vec{x})$ can be decomposed as

$$\epsilon_m(\vec{x}) = {}^4\mathbb{A}_m(\vec{x}) : \epsilon_M + \sum_{r=1}^N {}^4\mathbb{D}_r(\vec{x}) : \epsilon_r^{an} \quad (79)$$

Here, ${}^4\mathbb{D}_r(\vec{x})$ are the fourth-order tensors obtained by solving the problem (74)–(76) for $\epsilon_M = \mathbf{0}$ and for unitary components of ϵ_r^{an} . Using (76) and taking the spatial average over Ω , the macroscopic constitutive law is expressed by

$$\sigma_M = {}^4\mathbb{C}_M : \epsilon_M + \sum_{r=1}^N {}^4\mathbb{D}_{Mr} : \epsilon_r^{an} \quad (80)$$

where

$${}^4\mathbb{C}_M = \langle {}^4\mathbb{C}_m(\vec{x}) : {}^4\mathbb{A}_m(\vec{x}) \rangle \quad (81)$$

and

$${}^4\mathbb{D}_{Mr} = \langle {}^4\mathbb{C}_m(\vec{x}) : \{ {}^4\mathbb{D}_r(\vec{x}) - \chi^{(r)}(\vec{x}) {}^4\mathbb{I} \} \rangle \quad (82)$$

where ${}^4\mathbb{I}$ is the fourth-order identity tensor. The macroscopic stress depends only on a finite number, N , of internal variables, whose evolution is given in Michel and Suquet (2003).

It has been shown that the TFA method provides low accuracy in practice (Suquet, 1997b). One strategy to improving accuracy is to increase the number of subdomains in each phase (i.e., the number of eigenstrains in each phase), but at a price of increasing the number of internal state variables.

The nonuniform transformation analysis, NTFA, Michel and Suquet (2003) replaces the decomposition (78) by an expansion where anelastic eigenstrains $e_k^{an}(\vec{x})$ are spatially nonuniform:

$$\epsilon_m^{an}(\vec{x}) = \sum_{k=1}^P e_k^{an}(\vec{x}) \alpha_k \quad (83)$$

where α_k are scalar coefficients. This decomposition is completed by several assumptions on the anelastic modes, like incompressibility of plastic modes ($\text{tr}(e_r^{an}(\vec{x})) = 0$) and orthonormality of modes:

$$\langle e_s^{an}(\vec{x}) : e_r^{an}(\vec{x}) \rangle = 0, \quad s \neq r, \quad \langle (e_r^{an})_{eq} \rangle = 1 \quad (84)$$

where $(e)_{eq} = \left(\frac{2}{3} e : e \right)^{1/2}$. The anelastic modes $e_k^{an}(\vec{x})$ can be determined by numerical simulations where characteristic loads are prescribed on the RVE. An efficient method to select anelastic modes is the proper orthogonal decomposition, POD (Holmes *et al.*, 1996), which allows for extracting suitable modes from a collection of samples (Roussette *et al.*, 2009). A model has been proposed in Michel and Suquet (2003) to describe the evolution of internal variables. The strain fields can then be expressed as

$$\epsilon_m(\vec{x}) = {}^4\mathbb{A}_m(\vec{x}) : \epsilon_M + \sum_{k=1}^P \mathbf{D}_k(\vec{x}) \alpha_k \quad (85)$$

where $\mathbf{D}_k(\vec{x})$ are second-order strain tensors solutions of (74)–(76) taking in (83) $[e_k^{an}]^{(ij)} = \vec{e}_i \otimes \vec{e}_j$ for $k = R$, $[e_k^{an}] = \mathbf{0}$ for $k = 1, 2, \dots, N, k \neq R$. Using (85) and (83), we obtain the expression for the local Cauchy stress tensor:

$$\sigma_m(\vec{x}) = {}^4\mathbb{C}_m(\vec{x}) : \left[{}^4\mathbb{A}_m(\vec{x}) : \epsilon_M + \sum_{k=1}^P \mathbf{D}_k(\vec{x}) \alpha_k - \sum_{k=1}^P e_k^{an}(\vec{x}) \alpha_k \right] \quad (86)$$

Taking the spatial average over Ω , the effective constitutive law is given by

$$\sigma_M = {}^4\mathbb{C}_M : \epsilon_M + \sum_{k=1}^P \sigma_{Mk}^p \alpha_k \quad (87)$$

where ${}^4\mathbb{C}_M$ is the effective elastic modulus defined by (81) and

$$\sigma_{Mk} = \langle {}^4\mathbb{C}_m(\vec{x}) : [\mathbf{D}_k(\vec{x}) - e_k^{an}(\vec{x})] \rangle \quad (88)$$

6.4 Selection of plastic modes by POD

The choice of anelastic modes in the decomposition (83) is a critical component in the procedure to reduce the number of internal variables. In Michel and Suquet (2003), these modes were defined as sampled plastic strains obtained by preliminary simulations on the RVE. In that case, the modes are not orthogonal and it is difficult to select them and still reduce the number of modes. In Roussette *et al.* (2009),

the same authors have proposed to use a POD procedure, (Pearson, 1901; Schmidt, 1907; Lumley, 1967) to select the modes, which is briefly reminded below.

Considering a D -dimensional domain associated with a microstructure, subjected to a time-dependent quasi-static loading during a time interval $I = [0, T]$ discretized by S instants $\{t_1, t_2, \dots, t_S\}$, let \underline{q}_i denote the $D \times N$ -dimensional column formed by the displacement components of N points of the solid recorded at an instant $t_i \in I$. Considering a time-dependent vector $\underline{q}^R(t) \in \mathfrak{R}^{D \times N}$ and the following expansion:

$$\underline{q}^R(t) = \underline{\phi}_0 + \sum_{m=1}^P \underline{\phi}_m \xi_m(t) \quad (89)$$

with $M < D \times P$, $\underline{\phi}_0$ and $\underline{\phi}_m$ ($m = 1, \dots, P$) constant columns belonging to $\mathfrak{R}^{D \times N}$ and $\xi_m(t)$ scalar functions of time t . The time-dependent columns $\underline{q}^R(t)$ given by (89) are required to minimize:

$$\sum_{i=1}^S \|\underline{q}(t_i) - \underline{q}^R(t_i)\|^2 \quad (90)$$

with the constraints:

$$\langle \underline{\phi}_i, \underline{\phi}_j \rangle = \delta_{ij} \quad (91)$$

Solving this constrained optimization problem gives $\underline{\phi}_0$ as

$$\underline{\phi}_0 = \bar{\underline{q}} = \frac{1}{S} \sum_{i=1}^S \underline{q}(t_i) \quad (92)$$

and $\underline{\phi}_i$ ($i = 1, \dots, D \times N$) as the eigenvectors of the eigenvalue problem

$$\underline{Q} \underline{\phi}_i = \lambda_i \underline{\phi}_i \quad (93)$$

Here, \underline{Q} is the covariance matrix defined by

$$\underline{Q} = \underline{U} \underline{U}^T \quad (94)$$

where \underline{U} is a $((D \times N) \times S)$ matrix with centered columns:

$$\underline{U} = \{\underline{q}(t_1) - \bar{\underline{q}}, \underline{q}(t_2) - \bar{\underline{q}}, \dots, \underline{q}(t_S) - \bar{\underline{q}}\} \quad (95)$$

Note that \underline{Q} is a semidefinite $((D \times N) \times (D \times N))$ matrix, whose eigenvalues λ_i are decreasingly ordered: $\lambda_1 \geq \lambda_2 \geq \dots \geq \lambda_M \geq \dots \geq \lambda_{D \times N} \geq 0$.

A reduced model can be obtained using only a small number P of basis functions in (89). If $M < D \times N$, it can be shown (Liang *et al.*, 2002) that the error induced by the

POD procedure is given by

$$\epsilon(P) = \sum_{i=1}^S \|\underline{q}(\bar{\underline{x}}, t_i) - \underline{q}^R(\bar{\underline{x}}, t_i)\| = \left(\sum_{i=P+1}^{D \times N} \lambda_i \right)^{1/2} \quad (96)$$

The number of basis functions P is then chosen such that

$$\frac{\left(\sum_{i=P+1}^{D \times N} \lambda_i \right)^{1/2}}{\left(\sum_{i=1}^{D \times N} \lambda_i \right)^{1/2}} < \epsilon \quad (97)$$

where ϵ is a given tolerance error parameter, small compared to one.

In the case of quasi-static nonlinear problems, the eigenvalues in (96) quickly decrease, then a small number of associated eigenmodes can be selected to form a basis for reduced order models, for example, in the NTFA method described above. An illustration of results obtained by NTFA in Roussette *et al.* (2009) is provided in Figure 9.

7 PARALLEL IMPLEMENTATIONS AND HIGH-PERFORMANCE MULTISCALE COMPUTING

In this section, we describe an efficient and scalable parallel implementation of the CH framework that enables fully coupled multiscale simulations of failure (frequently spanning more than $\mathcal{O}(10^6)$ length scales) in engineering scale structures. High-performance computing (HPC) is a key enabling technology for both business and science. HPC is used in tackling grand societal challenges and has direct and measurable benefits on increasing global competitiveness and improving national economies (Sawyer and Parsons, 2011; NRC, 2012). We demonstrate the capability and performance of the proposed multiscale solver in the context of multiscale modeling of heterogeneous layers.

7.1 Hierarchically parallel framework for computational homogenization

A hierarchically parallel multiscale solver achieves ideal scalability by exploiting the inherent parallelism of CH and efficiently computing both the macroscale and microscale equilibrium in parallel using HPC platforms. Due to the separation of scales in CH (Figure 10), the response of each RUC may be computed independently, providing high parallelism in computing the fully coupled multiscale response.

The hierarchically parallel scheme uses a parallel finite element solver, *PGFem3D* (Matouš and Maniatty, 2004,

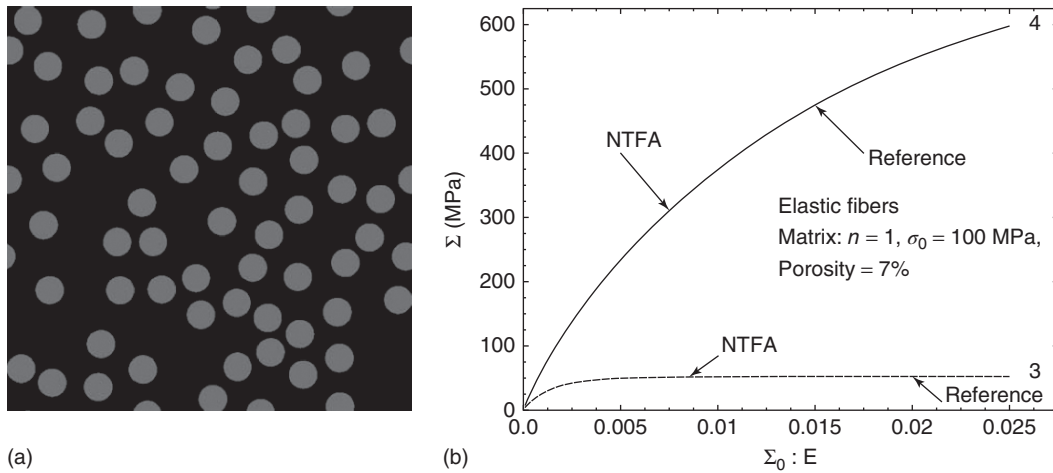


Figure 9. Randomly distributed fibers. Elastic fibers and porous elastic–viscoplastic matrix: (a) microstructure and (b) effective response of the composite. (Reproduced from Roussette *et al.* (2009).)

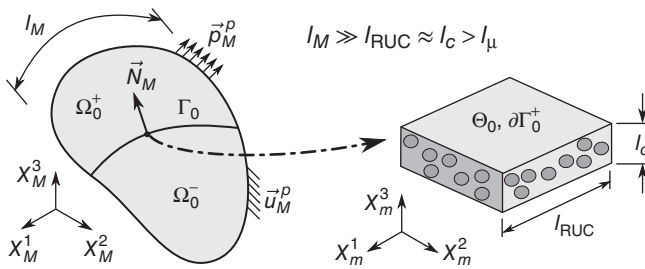


Figure 10. Separation of scales in the context of multiscale modeling of heterogeneous layers. l_M is the dimension of the macroscale interface, l_{RUC} is the size/width of the RUC (right) given as l_m in (5), l_c is the thickness of the heterogeneous layer, and l_μ is the scale of microfluctuations within the microstructure.

2009; Matouš and Geubelle, 2006; Mosby and Matouš, 2015a,b, 2016), at both scales and employs a client–server coupling for passing information between the macro and micro levels. The macroscale equilibrium is computed in parallel on the “client” processors, and the contributions from the individual RUCs are computed in parallel on the “servers” (see (5) and Figure 11a). The client–server communication is based on the message-passing interface (MPI) (MPI Forum, 2012), and different MPI communicators are used to reduce and simplify transmissions between and among the scales (Figure 11b). Communication is performed using dynamic point-to-point nonblocking messages and is efficiently overlaid with computation at both scales (for details, see Mosby and Matouš, 2015a).

Inhomogeneous macroscopic loading can lead to workload imbalance between the microscale servers due to some RUCs requiring more computational effort than others. In

addition, integrating the nonlinear evolution equations of the microscale constitutive models, for example, damage or plasticity, can further increase the workload imbalance between servers. This imbalance can lead to reduction in resource utilization and computational efficiency, wasting energy, and requiring longer simulations. These negative effects can be mitigated by redistributing the RUC computations on each server at the beginning of macroscale nonlinear iterations. A load-balancing algorithm can be used to reassign RUCs to servers based on how long the previous computations required. If the new assignment results in a more balanced server workload (i.e., the servers are predicted to complete all computations at approximately the same time), then the RUC state information is communicated to its newly assigned server. The RUC information is migrated between servers using nonblocking messages and is overlaid with computation of other RUCs that are not reassigned.

7.2 Numerical examples

We now present three numerical examples that demonstrate the performance and applicability of the hierarchically parallel CH solver. The efficient implementation of the CH solver enables computation of very large multiscale problems with high numerical resolution using a wide range of computational resources. With increasing availability of HPC resources, this method has great potential for advancing predictive computational materials science.

7.2.1 Scaling performance

One important aspect of multiscale modeling is computational performance of the numerical scheme. Typically,

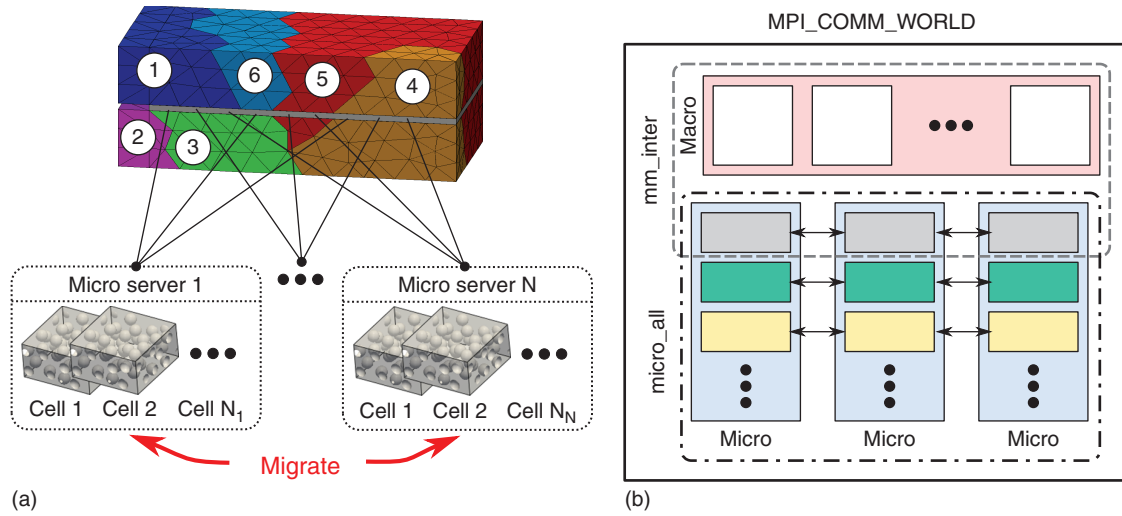


Figure 11. Schematic of the hierarchically parallel communication framework: (a) overview of the client–server structure and (b) schematic of the MPI communicators used to transmit information.

computational performance is measured in terms of “strong” and “weak” scaling. Strong scaling measures the computational speedup resulting from using more resources (i.e., computing cores) to compute the same simulation. Ideally, an increase in the number of computing cores results in a corresponding proportional decrease in computational time. Weak scaling measures the parallel efficiency by increasing the simulation size and computational resources in equal proportion, while comparing the time of computation. For more information on HPC aspects, see Hager and Wellein (2010).

The hierarchically parallel multiscale solver takes advantage of both of these scaling modes at each length scale. The macroscale domain can be solved on the optimal number of computing cores for its size, while the size of the microscale servers can be optimized for the available computational resources and/or the size and number of RUCs. Due to the separation of scales, the total number of computing cores is not limited by the strong or weak scaling performance of the solver at either length scale. Furthermore, due to the high overlay of computation and communication, as well as the relatively small size and number of communications between the scales, the CH algorithm performs ideally in the strong scaling sense with increasing numbers of microscale servers.

In particular, we demonstrate this ideal scaling behavior through simulation of a patch test (see schematic inset of Figure 12) using the Vulcan supercomputer at Lawrence Livermore National Laboratory (LLNL) (Mosby and Matouš, 2016).

The macroscale consists of two steel cubic adherends with $L = 10$ mm on each side separated by an interface.

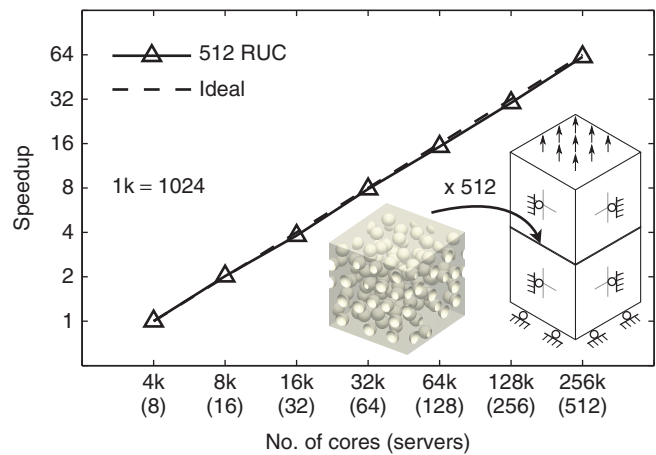


Figure 12. Strong scaling performance of the hierarchically parallel multiscale solver for the patch test shown in the inset. The complete multiscale simulation contains 747M finite elements and 396M DOFs. This scaling study was performed using the Vulcan machine at LLNL (from Mosby and Matouš, 2016).

The interface is discretized with 512 cohesive elements, each with a corresponding RUC. The RUC is $210 \times 210 \times 210 \mu\text{m}^3$ and is modeled as an epoxy resin containing 98 randomly distributed voids with $d = 30 \mu\text{m}$ ($c_p \approx 0.15$). The adhesively bonded structure is incrementally loaded in the vertical direction by a prescribed uniform displacement. The macroscale contains a total of 17.5k finite elements and 9.8k nonlinear degrees of freedom (DOFs), and is computed using 32 computing cores. The microscale RUCs each contain 1.46M finite elements and 773k nonlinear DOFs, and are computed on microservers using 512 computing cores each.

The time to compute the nonlinear solution for one fully coupled multiscale load increment is used to measure the strong scaling performance, and is shown in Figure 12 using 4096 up to 262 144 computing cores.

7.2.2 Large-scale simulation

We now demonstrate the capability of the hierarchically parallel solver to conduct extremely large simulations spanning $\mathcal{O}(10^5 - 10^6)$ length scales in a 3D finite strain setting (Mosby and Matouš, 2016). Figure 13 shows the results of a multiscale simulation for compression of a hyperelastic heterogeneous layer. The macroscale consists of two disks with $d = 20$ mm and $t = 10$ mm separated by a thin layer. Each macroscopic material point in the layer is represented by an RUC that is geometrically identical to the one in the previous section (Section 7.2.1). The top and bottom disks are constrained with a no-slip condition and are incrementally compressed by a prescribed displacement (see top left of Figure 13). The macroscale adherends are discretized with 320k finite elements, while the interface is discretized with 5296 cohesive elements (corresponding to 5296 RUCs). The macroscale contains a total of 182k nonlinear DOFs and is computed using 512 cores. The microscale RUCs are discretized with 10.2M finite elements ($h_{\min} = 191$ nm, $h_{\text{mean}} = 1.8$ μm , and $h_{\max} = 2.8$ μm) and 5.3M DOFs each, and are computed using microservers

of 512 cores each. The total implicit multiscale simulation contains 53.8B finite elements, 28.1B nonlinear DOFs, and was computed using 393 216 computing cores (786 432 threads) on the Vulcan machine at LLNL. Figure 13 shows the microscale response of two points on the macroscale interface (lower left), the response of the macroscale adherends (top right), and the macroscale response of the interface (lower right) at the end of the load history. As shown, the nonuniform response at both scales is captured.

7.2.3 Progressive failure of a dual cantilever beam

As previously discussed, the introduction of more complex physics and/or boundary conditions can lead to computational imbalance that results in degradation of the computational performance. To demonstrate this, we simulate the multiscale mode-I failure of a dual cantilever beam (DCB) shown in Figure 14. The DCB adherends are each 42-mm long, 10-mm wide, and 5-mm thick and are discretized with a total of 10k finite elements. The macroscale interface is 40-mm long (2-mm precrack) and is discretized by 322 cohesive elements. Each corresponding RUC is $250 \times 250 \times 125$ μm^3 and contains 40 randomly distributed voids with $d = 40$ μm . Failure within the RUC is modeled using a viscous isotropic damage model (Simo and Ju, 1989; Matouš *et al.*, 2008). The RUCs are each discretized with 249k finite elements, and the total multiscale simulation contains 80M finite elements and 42.5M nonlinear DOFs. The multiscale response is computed using up to 128k cores on the Mira supercomputer at Argonne National Laboratory. Figure 14 shows the fully coupled multiscale progressive failure response of the DCB. This multiscale response is compared to the Linear Fracture Mechanics (LFM) theory in Figure 14(c) (broken lines).

In this example, computational load imbalance is introduced by the more complex constitutive model at the microscale and the additional expense of integrating the material damage law in RUCs along the moving crack front. Therefore, RUCs associated with macroscale points in the macroscale damage process zone require more computational effort than those where the microscale damage is not evolving. One measure of the load imbalance is the maximum difference in time for all microservers to compute their assigned RUCs. Figure 14(d) shows the computational imbalance for the DCB simulation with and without the load-balancing algorithm. This algorithm immediately reduces the load imbalance introduced by integrating the damage law. Moreover, the average imbalance is reduced by nearly 40%, and the simulation is computed 12% faster overall.

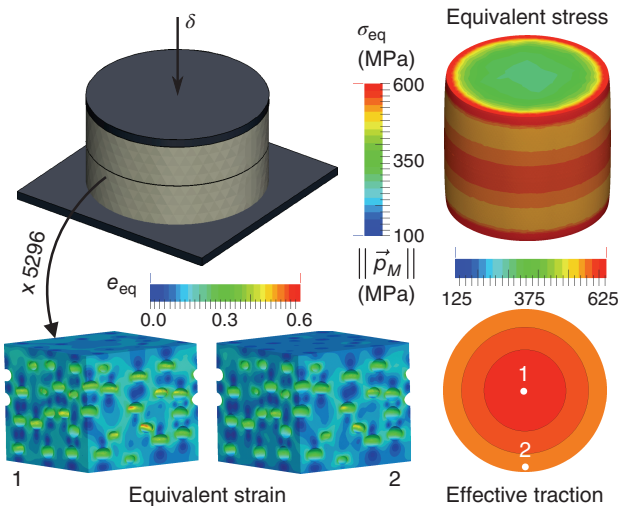


Figure 13. Large multiscale simulation of a heterogeneous hyperelastic layer under compression. Clockwise from top left: schematic of the macroscale domain and loading conditions, response of the macroscale adherends, macroscopic response of the interface, and microscale response of the heterogeneous interfaces at the marked points. This simulation was performed using the Vulcan machine at LLNL (from Mosby and Matouš, 2016).

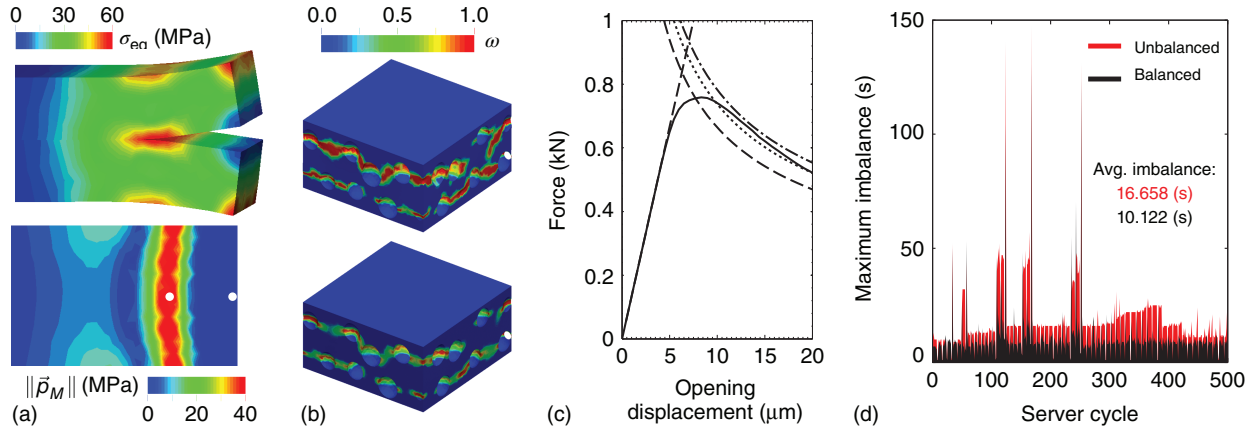


Figure 14. Fully coupled multiscale simulation of progressive mode-I failure of a DCB: (a) the macroscale response, (b) extent of damage in the microscale at the marked points in (a), (c) multiscale force–displacement curve, and (d) effect of the load-balancing algorithm. Broken lines in (c) denote the LFM theory response for $G_c^{\min} = 141 \text{ J/m}^2$ (dashed), $G_c^{\max} = 175 \text{ J/m}^2$ (dash-dot), and $G_c^{\text{mean}} = 162 \text{ J/m}^2$ (dotted) (from Mosby and Matouš, 2016).

8 CONCLUDING REMARKS

In spite of the progress made over the past decades, a lot of work still remains to be done in the broad field of multiscale computational engineering. Among the ongoing and expected trends and challenges, the following ones are highlighted:

- *3D, the third dimension (Section 7):* Most applications focus on two-dimensional descriptions of the considered materials with their governing deformation mechanisms. Without any doubt, more realistic three-dimensional computations and experimental analyses will be necessary, for example, Shan and Gokhale (2001) and Mosby and Matouš (2015a). The progress to be made here is evidently coupled to the increase in computational power in the coming decade(s).
- *Model reduction:* The high computational cost of nonlinear multiscale solution methods calls for novel efficient approaches that adequately balance computational speed and accuracy. The further development of model reduction techniques in combination with nonlinear multiscale schemes will be a necessity to make further progress.
- *Interaction with materials science, physics, and mathematics:* The various cross sections presented in this overview have clearly illustrated the growing interaction with materials science. The need for more accurate microstructural deformation models goes hand in hand with the need for more physics in the applied models. At the micron scale and even more at smaller scales, interaction with other physical phenomena is of major importance. It is expected that this trend will become

more pronounced in the near future. As mentioned in Section 1, multiscale methods are of general importance and attract attention from all fields in science and engineering. In particular, the developments in the physics community and the computational mathematics community are quite relevant for the nonlinear mechanics of materials. Increasing the interaction with these neighboring fields may speed up the developments considerably.

- *Multiscale versus multiple scales:* There is a growing interest in establishing correct scale transitions for various nonlinear problems in mechanics of materials, where in the mean time some problems are probably best tackled by considering multiple scales in a single domain. Challenges remain in both, where the most challenging example is probably to transition from damage to fracture across all length scales.
- *Temporal scale transitions:* Besides spatial scales, a lot more attention has to be given to temporal scales. Engineering approaches easily resort to accelerated tests to assess the lifetime of a material in a particular application. Many small-scale deformation mechanisms are characterized by typical time scales, which cannot be altered. Accelerated testing is therefore not always an adequate tool, since it may inhibit certain small-scale deformation processes. The proper incorporation of various (extreme) time scales in multiscale models therefore remains a challenge. Methods like the GENERIC scheme (Öttinger, 2005; Hütter and Tervoort, 2008b) offer clear opportunities in this sense.

ACKNOWLEDGMENTS

KM was supported in part by the U.S. Department of Energy, National Nuclear Security Administration as part of the Predictive Science Academic Alliance Program, under contract no. DE-NA0002377. KM would like to acknowledge resources of the Argonne Leadership Computing Facility under ALCC project number CSC188. KM would like to thank two of his graduate research assistants, M. Mosby and A. Gillman, for their numerous contributions to the multiscale modeling work presented in this chapter.

NOTES

1. The traction boundary conditions are not considered in the following, as they do not fit into the deformation-driven procedure. The minimal kinematic boundary conditions can be implemented along the same lines as discussed here for the periodic boundary conditions.

REFERENCES

- Abdulle A, Weinan E, Engquist B and Vanden-Eijnden E. The heterogeneous multiscale method. *Acta Numer.* 2012; **21**:1–87.
- Agoras P and Ponte Castañeda P. Homogenization estimates for multi-scale nonlinear composites. *Eur. J. Mech. A/Solids* 2011; **30**(6):828–843.
- Ahuja S, Yakhot V and Kevrekidis IG. Computational coarse graining of a randomly forced one-dimensional burgers equation. *Phys. Fluids* 2008; **20**(3): Article 035111.
- Babuška I. Homogenization and its application: mathematical and computational problems. In *Numerical Solution of Partial Differential Equations, III Synspade*, Hubbard B (ed.). Academic Press, 1976; 89–116.
- Babuška I. Solution of interface problems by homogenization - III. *SIAM J. Math. Anal.* 1977; **8**(6):923–937.
- Bacigalupo A and Gambarotta L. Nonlocal computational homogenization of periodic masonry. *Int. J. Multiscale Comput. Eng.* 2011; **9**(5):565–587.
- Beex LAA, Peerlings RHJ and Geers MGD. A multiscale quasi-continuum method for lattice models with bond failure and fiber sliding. *Comput. Methods Appl. Mech. Eng.* 2014a; **269**:108–122.
- Beex LAA, Peerlings RHJ and Geers MGD. A multiscale quasi-continuum method for dissipative lattice models and discrete networks. *J. Mech. Phys. Solids* 2014b; **64**:154–169.
- Belytschko T, Loehnert S and Song JH. Multiscale aggregating discontinuities: a method for circumventing loss of material stability. *Int. J. Numer. Methods Eng.* 2008; **73**(6):869–894.
- Bensoussan A, Lions J-L and Papanicoulau G. *Asymptotic Analysis for Periodic Structures*. North-Holland: Amsterdam, New York, Oxford, 1978.
- Binder K and Heermann DW. *Monte Carlo Simulation in Statistical Physics: An Introduction, Series in Solid-State Sciences*, vol. 80, Springer-Verlag, 1998.
- Bochenek B and Pyrz R. Reconstruction of random microstructures – a stochastic optimization problem. *Comput. Mater. Sci.* 2004; **31**(1):93–112.
- Bosco E, Kouznetsova VG, Coenen EWC, Geers MGD and Salvadori A. A multiscale framework for localizing microstructures towards the onset of macroscopic discontinuity. *Comput. Mech.* 2014; **54**(2):299–319.
- Bosco E, Kouznetsova VG and Geers MGD. Multi-scale computational homogenization–localization for propagating discontinuities using X-FEM. *Int. J. Numer. Methods Eng.* 2015; **102**(3–4):496–527.
- Chandler D. *Introduction to Modern Statistical Mechanics*. Oxford University Press: New York; 1987.
- Clément A, Soize C and Yvonnet J. Computational nonlinear stochastic homogenization using a non-concurrent multiscale approach for hyperelastic heterogeneous microstructures analysis. *Int. J. Numer. Methods Eng.* 2012; **91**(8):799–824.
- Coenen EWC, Kouznetsova VG and Geers MGD. Computational homogenization for heterogeneous thin sheets. *Int. J. Numer. Methods Eng.* 2010; **83**(8–9):1180–1205.
- Coenen EWC, Kouznetsova VG and Geers MGD. Multi-scale continuous-discontinuous framework for computational-homogenization-localization. *J. Mech. Phys. Solids* 2012a; **60**(8):1486–1507.
- Coenen EWC, Kouznetsova VG, Bosco E and Geers MGD. A multi-scale approach to bridge microscale damage and macroscale failure: a nested computational homogenization-localization framework. *Int. J. Fract.* 2012b; **178**(1–2):157–178.
- Coenen EWC, Kouznetsova VG and Geers MGD. Novel boundary conditions for strain localization analyses in microstructural volume elements. *Int. J. Numer. Methods Eng.* 2012c; **90**(1):1–21.
- Collins BC, Matous K and Rypil D. Three-dimensional reconstruction of statistically optimal unit cells of multimodal particulate composites. *Int. J. Multiscale Comput. Eng.* 2010; **8**(5):489–507.
- Cong Y, Nezamabadi S, Zahrouni H and Yvonnet J. Multiscale computational homogenization of heterogeneous shells at small strains with extensions to finite displacements and buckling. *Int. J. Numer. Methods Eng.* 2015, DOI: 10.1002/nme.4927.
- Curtin WA and Miller RE. Atomistic/continuum coupling in computational materials science. *Modell. Simul. Mater. Sci. Eng.* 2003; **11**:R33–R68.
- De Lorenzis L and Wriggers P. Computational homogenization of rubber friction on rough rigid surfaces. *Comput. Mater. Sci.* 2013; **77**:264–280.
- Doghri I and Friebel C. Effective elasto-plastic properties of inclusion-reinforced composites. Study of shape, orientation and cyclic response. *Mech. Mater.* 2005; **37**(1):45–68.
- Doghri I, Brassart L, Adam L and Gerard JS. A second-moment incremental formulation for the mean-field homogenization of elasto-plastic composites. *Int. J. Plast.* 2011; **27**(3):352–371.

- Drugan WJ and Willis JR. A micromechanics-based nonlocal constitutive equation and estimates of representative volume element size for elastic composites. *J. Mech. Phys. Solids* 1996; **44**(4):497–524.
- Duvaut G. Homogénéisation d'une classe de problèmes non linéaires. *C.R. Acad. Sci.* 1979; **A288**:775–778.
- Dvorak GJ. Transformation field analysis of inelastic composite materials. *Proc. R. Soc. London, Ser. A* 1992; **437**:311–327.
- Ebinger T, Steeb H and Diebels S. Modeling macroscopic extended continua with the aid of numerical homogenization schemes. *Comput. Mater. Sci.* 2005; **32**(3–4):337–347.
- Ehlers W, Ramm E, Diebels S and D'Addetta GA. From particle ensembles to Cosserat continua: homogenization of contact forces towards stresses and couple stresses. *Int. J. Solids Struct.* 2003; **40**(24):6681–6702.
- Eshelby JD. The determination of the elastic field of an ellipsoidal inclusion. *Proc. R. Soc. London, Ser. A* 1957; **241**:376–396.
- Feyel F and Chaboche J-L. FE² multiscale approach for modelling the elasto-viscoplastic behaviour of long fibre SiC/Ti composite materials. *Comput. Methods Appl. Mech. Eng.* 2000; **183**:309–330.
- Fillep S, Mergheim J and Steinmann P. Computational homogenization of rope-like technical textiles. *Comput. Mech.* 2015; **55**(3):577–590.
- Fish J. Bridging the scales in nano engineering and science. *J. Nanopart. Res.* 2006; **8**:577–594.
- Fish J (ed.) *Multiscale Methods: Bridging the Scales in Science and Engineering*. Oxford University Press: Oxford, 2009.
- Fish J and Fan R. Mathematical homogenization of nonperiodic heterogeneous media subjected to large deformation transient loading. *Int. J. Numer. Methods Eng.* 2008; **76**(7):1044–1064.
- Fish J and Kuznetsov S. Computational continua. *Int. J. Numer. Methods Eng.* 2010; **84**(7):774–802.
- Fish J, Shek K, Pandheeradi M and Shephard MS. Computational plasticity for composite structures based on mathematical homogenization: theory and practice. *Comput. Methods Appl. Mech. Eng.* 1997; **148**(1–2):53–73.
- Fish J, Filonova V and Yuan Z. Hybrid impotent-incompatible eigenstrain based homogenization. *Int. J. Numer. Methods Eng.* 2013; **95**(1):1–32.
- Fish J, Filonova V and Fafalis D. Computational continua revisited. *Int. J. Numer. Methods Eng.* 2015; **102**(3–4):332–378.
- Forest S, Pradel F and Sab K. Asymptotic analysis of heterogeneous Cosserat media. *Int. J. Solids Struct.* 2001; **38**:4585–4608.
- Fritzen F and Boehlke T. Nonuniform transformation field analysis of materials with morphological anisotropy. *Compos. Sci. Technol.* 2011; **71**(4):433–442.
- Fritzen F and Leuschner M. Reduced basis hybrid computational homogenization based on a mixed incremental formulation. *Comput. Methods Appl. Mech. Eng.* 2013; **260**:143–154.
- Fritzen F, Hodapp M and Leuschner M. Gpu accelerated computational homogenization based on a variational approach in a reduced basis framework. *Comput. Methods Appl. Mech. Eng.* 2014; **278**:186–217.
- Garikipati K and Hughes TJR. A variational multiscale approach to strain localization - formulation for multidimensional problems. *Comput. Methods Appl. Mech. Eng.* 2000; **188**(1–3):39–60.
- Geers MGD, Kouznetsova VG and Brekelmans WAM. Gradient-enhanced computational homogenization for the micro-macro scale transition. *J. Phys. IV* 2001; **11**(5):5145–5152.
- Geers MGD, Kouznetsova VG and Brekelmans WAM. Multi-scale second-order computational homogenization of microstructures towards continua. *Int. J. Multiscale Comput. Eng.* 2003; **1**(4):371–386.
- Geers MGD, Coenen EWC and Kouznetsova VG. Multi-scale computational homogenization of structured thin sheets. *Modell. Simul. Mater. Sci. Eng.* 2007; **15**:S393–S404.
- Geers MGD, Kouznetsova VG and Brekelmans WAM. Multi-scale computational homogenization: trends & challenges. *J. Comput. Appl. Math.* 2010; **234**(7):2175–2182.
- Germain P. Continuum thermodynamics. *J. Appl. Mech.* 1983; **50**:1010–1020.
- Ghosh S, Lee K and Moorthy S. Two scale analysis of heterogeneous elastic-plastic materials with asymptotic homogenization and Voronoi cell finite element model. *Comput. Methods Appl. Mech. Eng.* 1996; **132**:63–116.
- Ghosh S, Lee K and Raghavan P. A multi-level computational model for multi-scale damage analysis in composite and porous materials. *Int. J. Solids Struct.* 2001; **38**(14):2335–2385.
- Gillman A and Matouš K. Third-order model of thermal conductivity for random polydisperse particulate materials using well-resolved statistical descriptions from tomography. *Phys. Lett. A* 2014; **378**(41):3070–3073.
- Gillman A, Matouš K and Atkinson S. Microstructure-statistics-property relations of anisotropic polydisperse particulate composites using tomography. *Phys. Rev. E* 2013; **87**(2):022208-1–022208-19.
- Gillman A, Amadio G, Matouš K and Jackson TL. Third-order thermo-mechanical properties for packs of Platonic solids using statistical micromechanics. *Proc. R. Soc. London, Ser. A* 2015; **471**(2177):20150060-1–20150060-20.
- Gitman IM, Askes H and Sluys LJ. Coupled-volume multi-scale modelling of quasi-brittle material. *Eur. J. Mech. A Solids* 2008; **27**(3):302–327.
- Grmela M. Why GENERIC? *J. Non-Newtonian Fluid Mech.* 2010a; **165**:980–986.
- Grmela M. Multiscale equilibrium and nonequilibrium thermodynamics in chemical engineering. *Adv. Chem. Eng.* 2010b; **39**:75–129.
- Gurson AL. Continuum theory of ductile rupture by void nucleation and growth: Part I yield criteria and flow rules for porous ductile media. *J. Eng. Mater. Technol.* 1977; **99**(1):2–15.
- Hager G and Wellein G. *Introduction to High Performance Computing for Scientists and Engineers*. CRC Press, 2010.
- Halphen B and Nguyen Q. Sur les matériaux standards généralisés. *J. Méc.* 1975; **14**(1):39–63.
- Hashin Z. Viscoelastic behavior of heterogeneous media. *J. Appl. Mech.* 1965; **32**:630–636.
- Hashin Z. Complex moduli of viscoelastic composites - I. General theory and application to particulate composites. *Int. J. Solids Struct.* 1970; **6**:539–552.
- Hashin Z and Shtrikman S. A variational approach to the theory of the elastic behaviour of multiphase materials. *J. Mech. Phys. Solids* 1963; **11**:127–140.

- Helfen CE and Diebels S. Computational homogenisation of composite plates: consideration of the thickness change with a modified projection strategy. *Comput. Math. Appl.* 2014; **67**(5):1116–1129.
- Hettich T, Hund A and Ramm E. Modeling of failure in composites by X-FEM and level sets within a multiscale framework. *Comput. Methods Appl. Mech. Eng.* 2008; **197**(5):414–424.
- Hill R. Elastic properties of reinforced solids: some theoretical principles. *J. Mech. Phys. Solids* 1963; **11**(5):357–372.
- Hill R. Continuum micromechanics of elastoplastic polycrystals. *J. Mech. Phys. Solids* 1965; **13**:89–101.
- Holmes P, Lumley JL and Berkooz G. *Turbulence, Coherent Structures, Dynamical Systems and Symmetry*. Cambridge University Press: Cambridge, 1996.
- Hughes TJR, Feijóo GR, Mazzei L and Quincy J. The variational multiscale method - a paradigm for computational mechanics. *Comput. Methods Appl. Mech. Eng.* 1998; **166**:3–24.
- Hutchinson JW. Bounds and self-consistent estimates for creep of polycrystalline metals. *Proc. R. Soc. London, Ser. A* 1976; **394**:87–119.
- Hütter M and Tervoort TA. Finite anisotropic elasticity and material frame indifference from a nonequilibrium thermodynamics perspective. *J. Non-Newtonian Fluid Mech.* 2008a; **152**(1–3):45–52.
- Hütter M and Tervoort TA. Coarse graining in elasto-viscoplasticity: bridging the gap from microscopic fluctuations to dissipation. *Adv. Appl. Mech.* 2008b; **42**:253–317.
- Itchev A, Marcadon V, Kruch S and Forest S. Computational homogenisation of periodic cellular materials: application to structural modelling. *Int. J. Mech. Sci.* 2015; **93**:240–255.
- Inglis HM, Geubelle PH and Matouš K. Boundary condition effects on multiscale analysis of damage localization. *Philos. Mag.* 2008; **88**(16):2373–2397.
- Javili A, Chatzigeorgiou G and Steinmann P. Computational homogenization in magneto-mechanics. *Int. J. Solids Struct.* 2013; **50**(25–26):4197–4216.
- Kaczmarczyk L, Pearce CJ and Bicanic N. Scale transition and enforcement of RVE boundary conditions in second-order computational homogenization. *Int. J. Numer. Methods Eng.* 2008; **74**(3):506–522.
- Kaczmarczyk L, Pearce CJ and Bicanic N. Studies of microstructural size effect and higher-order deformation in second-order computational homogenization. *Comput. Struct.* 2010; **88**(23–24):1383–1390.
- Kanit T, Forest S, Galliet I, Mounoury V and Jeulin D. Determination of the size of the representative volume element for random composites: statistical and numerical approach. *Int. J. Solids Struct.* 2003; **40**:3647–3679.
- Kanit T, N’Guyen F, Forest S, Jeulin D, Reed M and Singleton S. Apparent and effective physical properties of heterogeneous materials: representativity of samples of two materials from food industry. *Comput. Methods Appl. Mech. Eng.* 2006; **195**:3960–3982.
- Keip MA, Steinmann P and Schröder J. Two-scale computational homogenization of electro-elasticity at finite strains. *Comput. Methods Appl. Mech. Eng.* 2014; **278**:62–79.
- Keller JB. A theorem on the conductivity of a composite medium. *J. Math. Phys.* 1964; **5**:548–549.
- Keller JB. Effective behavior of heterogeneous media. In *Statistical Mechanics and Statistical Methods in Theory and Application: A Tribute to Elliott W. Montroll*, Landman U (ed.). Plenum, 1977.
- Kerfriden P, Rodenas JJ and Bordas SPA. Certification of projection-based reduced order modelling in computational homogenisation by the constitutive relation error. *Int. J. Numer. Methods Eng.* 2014; **97**(6):395–422.
- Khisaeva ZF and Ostoja-Starzewski M. On the size of RVE in finite elasticity of random composites. *J. Elast.* 2006; **85**(2):153–173.
- Knap J and Ortiz M. An analysis of the quasicontinuum method. *J. Mech. Phys. Solids* 2001; **49**(9):1899–1923.
- Kouznetsova VG. *Computational homogenization for the multi-scale analysis of multi-phase materials*. PhD thesis, Eindhoven University of Technology, Mechanical Engineering Department, 2002.
- Kouznetsova VG, Brekelmans WAM and Baaijens FPT. An approach to micro-macro modeling of heterogeneous materials. *Comput. Mech.* 2001; **27**:37–48.
- Kouznetsova VG, Geers MGD and Brekelmans WAM. Advanced constitutive modeling of heterogeneous materials with a gradient-enhanced computational homogenization scheme. *Int. J. Numer. Methods Eng.* 2002; **54**:1235–1260.
- Kouznetsova VG, Geers MGD and Brekelmans WAM. Size of a representative volume element in a second-order computational homogenization framework. *Int. J. Multiscale Comput. Eng.* 2004a; **2**(4):575–598.
- Kouznetsova VG, Geers MGD and Brekelmans WAM. Multi-scale second-order computational homogenization of multi-phase materials: a nested finite element solution strategy. *Comput. Methods Appl. Mech. Eng.* 2004b; **193**:5525–5550.
- Kröner E. Berechnung der elastischen konstanten des vielkristalls aus den konstanten des einkristalls. *Z. Phys.* 1958; **151**:504–518.
- Kröner E. Zur plastischen verformung des vielkristalls. *Acta Metall.* 1961; **9**:155–161.
- Kulkarni MG, Geubelle PH and Matouš K. Multi-scale modeling of heterogeneous adhesives: effect of particle decohesion. *Mech. Mater.* 2009; **41**(5):573–583.
- Kulkarni MG, Matouš K and Geubelle PH. Coupled multi-scale cohesive modeling of failure in heterogeneous adhesives. *Int. J. Numer. Methods Eng.* 2010; **84**(8):916–946.
- Kumar H, Briant CL and Curtin WA. Using microstructure reconstruction to model mechanical behavior in complex microstructures. *Mech. Mater.* 2006; **38**:818–832.
- Kumar NC, Matouš K and Geubelle PH. Reconstruction of periodic unit cells of multimodal random particulate composites using genetic algorithms. *Comput. Mater. Sci.* 2008; **42**:352–367.
- Larsson F, Runesson K and Su F. Variationally consistent computational homogenization of transient heat flow. *Int. J. Numer. Methods Eng.* 2010; **81**(13):1659–1686.
- Larsson F, Runesson K, Saroukhani S and Vafadari R. Computational homogenization based on a weak format of micro-periodicity for RVE-problems. *Comput. Methods Appl. Mech. Eng.* 2011; **200**(1–4):11–26.
- Lee H, Brandyberry M, Tudor A and Matouš K. Three-dimensional reconstruction of statistically optimal unit cells of polydisperse particulate composites from microtomography. *Phys. Rev. E* 2009; **80**(6):061301-1–061301-12.

- Lee H, Gillman AS and Matouš K. Computing overall elastic constants of polydisperse particulate composites from microtomographic data. *J. Mech. Phys. Solids* 2011; **59**(9):1838–1857.
- Liang YC, Lee HP, Lim SP, Lin WZ and Lee KH. Proper orthogonal decomposition and its applications - part I: theory. *J. Sound Vib.* 2002; **3**:527–544.
- Lions J-L. Remarks on some asymptotic problems in composite materials and in perforated materials. In *Variational Methods in Mechanics of Solids*, Nemat-Nasser S (ed.). Pergamon Press, 1979.
- Liu WK, Karpov EG, Zhang S and Park HS. An introduction to computational nanomechanics and materials. *Comput. Methods Appl. Mech. Eng.* 2004; **193**:1529–1578.
- Liu XK, Liang YB, Duan QL, Schrefler BA and Du YY. A mixed finite element procedure of gradient cosserat continuum for second-order computational homogenisation of granular materials. *Comput. Mech.* 2014; **54**(5):1331–1356.
- Loehnert S and Belytschko T. A multiscale projection method for macro/microcrack simulations. *Int. J. Numer. Methods Eng.* 2007; **71**(12):1466–1482.
- Lumley JL. The structure of inhomogeneous turbulent flows. In *Atmospheric Turbulence and Radio Wave Propagation*, Yaglom AM and Tatarski VI (eds). Publishing House: Nauka, 1967; 166–178.
- Markenscoff X and Dascalu C. Asymptotic homogenization analysis for damage amplification due to singular interaction of micro-cracks. *J. Mech. Phys. Solids* 2012; **60**(8):1478–1485.
- Massart TJ, Peerlings RHJ and Geers MGD. An enhanced multi-scale approach for masonry wall computations with localization of damage. *Int. J. Numer. Methods Eng.* 2007a; **69**(5):1022–1059.
- Massart TJ, Peerlings RHJ and Geers MGD. Structural damage analysis of masonry walls using computational homogenization. *Int. J. Damage Mech.* 2007b; **16**:199–226.
- Matouš K and Geubelle PH. Multiscale modelling of particle debonding in reinforced elastomers subjected to finite deformations. *Int. J. Numer. Methods Eng.* 2006; **65**(2):190–223.
- Matouš K and Maniatty AM. Finite element formulation for modelling large deformations in elasto-viscoplastic polycrystals. *Int. J. Numer. Methods Eng.* 2004; **60**(14):2313–2333.
- Matouš K and Maniatty AM. Multiscale modeling of elasto-viscoplastic polycrystals subjected to finite deformations. *Interact. Multiscale Mech.* 2009; **2**(4):375–396.
- Matouš K, Kulkarni MG and Geubelle PH. Multiscale cohesive failure modeling of heterogeneous adhesives. *J. Mech. Phys. Solids* 2008; **56**(4):1511–1533.
- Mesarovic SD, Padbidri J. Minimal kinematic boundary conditions for simulations of disordered microstructures. *Philos. Mag.* 2005; **85**:65–76.
- Michel J-C and Suquet P. Nonuniform transformation field analysis. *Int. J. Solids Struct.* 2003; **40**(25):6937–6955.
- Miehe C. Numerical computation of algorithmic (consistent) tangent moduli in large-strain computational inelasticity. *Comput. Methods Appl. Mech. Eng.* 1996; **134**:223–240.
- Miehe C. Strain-driven homogenization of inelastic microstructures and composites based on an incremental variational formulation. *Int. J. Numer. Methods Eng.* 2002; **55**(11):1285–1322.
- Miehe C and Bayreuther CG. On multiscale FE analyses of heterogeneous structures: from homogenization to multigrid solvers. *Int. J. Numer. Methods Eng.* 2007; **71**(10):1135–1180.
- Miehe C and Koch A. Computational micro-to-macro transition of discretized microstructures undergoing small strain. *Arch. Appl. Mech.* 2002; **72**:300–317.
- Miehe C, Schröder J and Becker M. Computational homogenization analysis in finite elasticity: material and structural instabilities on the micro- and macro-scales of periodic composites and their interaction. *Comput. Methods Appl. Mech. Eng.* 2002; **191**(44):4971–5005.
- Miehe C, Schotte J and Schröder J. Computational micro-macro transitions and overall moduli in the analysis of polycrystals at large strains. *Comput. Mater. Sci.* 1999a; **16**(1–4):372–382.
- Miehe C, Schröder J and Schotte J. Computational homogenization analysis in finite plasticity. Simulation of texture development in polycrystalline materials. *Comput. Methods Appl. Mech. Eng.* 1999b; **171**:387–418.
- Milton GW. *The Theory of Composites*, vol. 6. Cambridge University Press: Cambridge, 2002.
- Moës N and Belytschko T. Extended finite element method for cohesive crack growth. *Eng. Fract. Mech.* 2002; **69**(7):813–833.
- Mori T and Tanaka K. Average stress in the matrix and average elastic energy of materials with misfitting inclusions. *Acta Metall.* 1973; **21**:571–574.
- Mosby M and Matouš K. Hierarchically parallel coupled finite strain multiscale solver for modeling heterogeneous layers. *Int. J. Numer. Methods Eng.* 2015a; **102**(3–4):748–765.
- Mosby M and Matouš K. On mechanics and material length scales of failure in heterogeneous interfaces using a finite strain high performance solver. *Modell. Simul. Mater. Sci. Eng.* 2015b; **23**:085014.
- Mosby M and Matouš K. Computational homogenization at extreme scales. *Extreme Mech. Lett.* 2016; **6**:68–74.
- MPI Forum. *A Message-Passing Interface Standard: Version 3.0*. University of Tennessee: Knoxville, TN, 2012.
- Nemat-Nasser S. Retrospect and prospect: micromechanics. In *Proceedings of the Ninth conference on Engineering Mechanics*, College Station, TX, 1992.
- Nemat-Nasser S and Hori M. *Micromechanics: Overall Properties of Heterogeneous Materials*. Elsevier: Amsterdam, 1993.
- Nemat-Nasser S and Obata M. Rate-dependent finite elasto-plastic deformation of polycrystals. *Proc. R. Soc. London, Ser. A* 1986; **407**:343–375.
- Nezamabadi S, Yvonnet J, Zahrouni H and Potier-Ferry M. A multi-level computational strategy for handling microscopic and macroscopic instabilities. *Comput. Methods Appl. Mech. Eng.* 2009; **198**(27–29):2099–2110.
- Nguyen VP, Lloberas-Valls O, Stroeven M and Sluys LJ. Computational homogenization for multiscale crack modeling. Implementational and computational aspects. *Int. J. Numer. Methods Eng.* 2012; **89**(2):192–226.
- Nguyen VD and Noels L. Computational homogenization of cellular materials. *Int. J. Solids Struct.* 2014; **51**(11–12):2183–2203.
- Nilenius F, Larsson F, Lundgren K and Runesson K. Computational homogenization of diffusion in three-phase mesoscale concrete. *Comput. Mech.* 2014; **54**(2):461–472.
- Niyonzima I, Sabariego RV, Dular P and Geuzaine C. Nonlinear computational homogenization method for the evaluation of eddy currents in soft magnetic composites. *IEEE Trans. Magn.* 2014; **50**(2): Article Number: 7001304.

- NRC. *A National Strategy for Advancing Climate Modeling*. The National Academy Press, 2012.
- Ohman M, Larsson F and Runesson K. Computational homogenization of liquid-phase sintering with seamless transition from macroscopic compressibility to incompressibility. *Comput. Methods Appl. Mech. Eng.* 2013; **266**:219–228.
- Ortiz M. Computational micromechanics. *Comput. Mech.* 1996; **18**(5):321–338.
- Ostoja-Starzewski M, Boccara SD and Jasiuk I. Couple-stress moduli and characteristic length of a two-phase composite. *Mech. Res. Commun.* 1999; **26**(4):387–396.
- Öttinger HC. *Beyond Equilibrium Thermodynamics*. John Wiley & Sons, Inc., 2005.
- Özdemir I, Brekelmans WAM and Geers MGD. Computational homogenization for heat conduction in heterogeneous solids. *Int. J. Numer. Methods Eng.* 2008a; **73**(2):185–204.
- Özdemir I, Brekelmans WAM and Geers MGD. FE² computational homogenization for the thermo-mechanical analysis of heterogeneous solids. *Comput. Methods Appl. Mech. Eng.* 2008b; **198**(3–4):602–613.
- Pearson K. On lines and planes of closest fit to systems of points in space. *Philos. Mag.* 1901; **6**:559.
- Peerlings RHJ and Fleck NA. Numerical analysis of strain gradient effects in periodic media. *J. Phys. IV* 2001; **11**:153–160.
- Perić D, de Souza Neto EA, Feijóo RA, Partovi M and Molina AJC. On micro-to-macro transitions for multi-scale analysis of non-linear heterogeneous materials: unified variational basis and finite element implementation. *Int. J. Numer. Methods Eng.* 2011; **87**(1–5):149–170.
- Pham K, Kouznetsova VG and Geers MGD. Transient computational homogenization for heterogeneous materials under dynamic excitation. *J. Mech. Phys. Solids* 2013; **61**(11):2125–2146.
- Plews JA and Duarte CA. Bridging multiple structural scales with a generalized finite element method. *Int. J. Numer. Methods Eng.* 2014; **102**(3–4):180–201.
- Ponte Castañeda P. The effective mechanical properties of nonlinear isotropic composites. *J. Mech. Phys. Solids* 1991; **39**:45–71.
- Ponte Castañeda P. New variational principles in plasticity and their application to composite materials. *J. Mech. Phys. Solids* 1992; **40**:1757–1788.
- Ponte Castañeda P. Three-point bounds and other estimates for strongly nonlinear composites. *Phys. Rev. B* 1998; **57**(19):12077–12083.
- Ponte Castañeda P. Second-order homogenization estimates for nonlinear composites incorporating field fluctuations: I Theory. *J. Mech. Phys. Solids* 2002; **50**(4):737–757.
- Ponte Castañeda P and Galipeau E. Homogenization-based constitutive models for magnetorheological elastomers at finite strain. *J. Mech. Phys. Solids* 2011; **59**(2):194–215.
- Povirk GL. Incorporation of microstructural information into models of two-phase materials. *Acta Metall. Mater.* 1995; **43**(8):3199–3206.
- Raabe D. *Computational Materials Science: The Simulation of Materials, Microstructures and Properties*. Wiley-VCH Verlag GmbH: Weinheim, 1998.
- Ridderbos K. The coarse-graining approach to statistical mechanics: how blissful is our ignorance? *Stud. Hist. Philos. Sci. Part B: Stud. Hist. Philos. Mod. Phys.* 2002; **33**(1):65–67.
- Roussette S, Michel JC and Suquet P. Non uniform transformation field analysis of elastic-viscoplastic composites. *Compos. Sci. Technol.* 2009; **69**:22–27.
- Sachs G. Zur ableitung einer fließbedingung. *Z. Ver. Dtsch. Ing.* 1928; **72**:734–736.
- Salvadori A, Bosco E and Grazioli D. A computational homogenization approach for Li-ion battery cells: part 1-formulation. *J. Mech. Phys. Solids* 2014; **65**:114–137.
- Sanchez-Palencia E. *Non-Homogeneous Media and Vibration Theory*, Lecture Notes in Physics, vol. 127. Springer-Verlag, 1980.
- Sawyer M and Parsons M (eds). *PlanetHPC: A Strategy for Research and Innovation through High Performance Computing*. University of Edinburgh: Edinburgh, 2011.
- Schmidt E. Zur theorie der linearen und nichtlinearen integralgleichungen. I Teil: Entwicklung willkürlicher funktion nach systemen vorgeschriebener. *Math. Ann.* 1907; **63**:433–476.
- Schröder J and Keip M-A. Two-scale homogenization of electromechanically coupled boundary value problems. *Comput. Mech.* 2012; **50**(2):229–244.
- Segurado J and Llorca J. Simulation of the deformation of polycrystalline nanostructured Ti by computational homogenization. *Comput. Mater. Sci.* 2013; **76**:3–11.
- Shan Z and Gokhale AM. Micromechanics of complex three-dimensional microstructures. *Acta Mater.* 2001; **49**(11):2001–2015.
- Simo JC and Ju JW. On continuum damage-elastoplasticity at finite strains. *Comput. Mech.* 1989; **5**(5):375–400.
- van der Sluis O, Vosbeek PHJ, Schreurs PJG and Meijer HEH. Homogenization of heterogeneous polymers. *Int. J. Solids Struct.* 1999; **36**:3193–3214.
- van der Sluis O, Schreurs PJG, Brekelmans WAM and Meijer HEH. Overall behaviour of heterogeneous elastoviscoplastic materials: effect of microstructural modelling. *Mech. Mater.* 2000; **32**:449–462.
- Smit RJM, Brekelmans WAM and Meijer HEH. Prediction of the mechanical behaviour of non-linear systems by multi-level finite element modeling. *Comput. Methods Appl. Mech. Eng.* 1998; **155**:181–192.
- Smyshlyayev VP and Cherednichenko KD. On rigorous derivation of strain gradient effects in the overall behaviour of periodic heterogeneous media. *J. Mech. Phys. Solids* 2000; **48**:1325–1357.
- Smyshlyayev VP and Fleck NA. Bounds and estimates for linear composites with strain gradient effects. *J. Mech. Phys. Solids* 1994; **42**(12):1851–1882.
- Su F, Larsson F and Runesson K. Computational homogenization of coupled consolidation problems in micro-heterogeneous porous media. *Int. J. Numer. Methods Eng.* 2011; **88**(11):1198–1218.
- Suquet PM. Local and global aspects in the mathematical theory of plasticity. In *Plasticity Today: Modelling, Methods and Applications*. Elsevier Applied Science Publishers; 1985a; 279–310.
- Suquet PM. Local and global aspects in the mathematical theory of plasticity. In *Plasticity Today: Modelling, Methods and Applications*, Sawczuk A and Bianchi G (eds). Elsevier Applied Science Publishers, 1985b; 279–310.

- Suquet PM. Elements of homogenization theory for inelastic solid mechanics. In *Homogenization Techniques for Composite Media*, Lecture Note on Physics, vol. 272, Sanchez-Palencia E and Zaoui A (eds). Springer-Verlag, 1987; 193–278.
- Suquet P. Overall potentials and extremal surfaces of power law or ideally plastic materials. *J. Mech. Phys. Solids* 1993; **41**:981–1002.
- Suquet P. *Continuum Micromechanics, CISM Courses and Lectures*, vol. 377. Springer-Verlag, 1997a.
- Suquet P. Effective properties for nonlinear composites. In *Continuum Micromechanics, International Centre for Mechanical Sciences*, vol. 377, Springer: Vienna, 1997b; 197–264.
- Tadmor EB, Ortiz M and Phillips R. Mixed atomistic and continuum models of deformation in solids. *Langmuir* 1996a; **12**(19):4529–4534.
- Tadmor EB, Phillips R and Ortiz M. Quasicontinuum analysis of defects in solids. *Philos. Mag.* 1996b; **A73**(6):1529–1563.
- Takano N, Zako M and Ohnishi Y. Macro-micro uncoupled homogenization procedure for microscopic nonlinear behavior analysis of composites. *Mater. Sci. Res. Int.* 1996; **2**(2):81–86.
- Talbot DRS and Willis JR. Variational principles for inhomogeneous non-linear media. *J. Appl. Math.* 1985; **35**(1):39–54.
- Taylor GI. Plastic strain in metals. *J. Inst. Met.* 1938; **62**:307–324.
- Temizer I. Multiscale thermomechanical contact: computational homogenization with isogeometric analysis. *Int. J. Numer. Methods Eng.* 2014a; **97**(8):582–607.
- Temizer I. Computational homogenization of soft matter friction: isogeometric framework and elastic boundary layers. *Int. J. Numer. Methods Eng.* 2014b; **100**(13):953–981.
- Temizer I and Wriggers P. An adaptive method for homogenization in orthotropic nonlinear elasticity. *Comput. Methods Appl. Mech. Eng.* 2007; **35–36**:3409–3423.
- Terada K and Kikuchi N. Nonlinear homogenization method for practical applications. In *Computational Methods in Micromechanics, Proceedings of the ASME International Mechanical Engineering Congress and Exposition, AMD-vol. 212/MD-vol. 62*, Ghosh S and Ostoja-Starzewski M (eds), American Society of Mechanical Engineers (ASME), USA, 1995; 1–6.
- Terada K and Kikuchi N. A class of general algorithms for multi-scale analyses of heterogeneous media. *Comput. Methods Appl. Mech. Eng.* 2001; **190**(40–41):5247–5464.
- Terada K, Hori M, Kyoya T and Kikuchi N. Simulation of the multi-scale convergence in computational homogenization approaches. *Int. J. Solids Struct.* 2000; **37**(16):2285–2311.
- Terada K, Kato J, Hirayama N, Inugai T and Yamamoto K. A method of two-scale analysis with micro-macro decoupling scheme: application to hyperelastic composite materials. *Comput. Mech.* 2013; **52**:1199–1219.
- Terada K, Hirayama N, Yamamoto K, Kato J, Kyoya T, Matsubara S, Arakawa Y, Ueno Y and Miyayama N. An adaptive method for homogenization in orthotropic nonlinear elasticity. *Adv. Compos. Mater.* 2014; **23**(5–6):421–450.
- Torrens IM. *Interatomic Potentials*. Academic Press: New York, 1972.
- Torquato S. *Random Heterogeneous Materials: Microstructure and Macroscopic Properties*, vol. 16. Springer Science & Business Media, 2002.
- Tran AB, Yvonnet J, He Q-C, Toulemonde C and Sanahuja J. A simple computational homogenization method for structures made of heterogeneous linear viscoelastic materials. *Comput. Methods Appl. Mech. Eng.* 2011; **200**(45–46):2956–2970.
- Triantafyllidis N and Bardenhagen S. The influence of scale size on the stability of periodic solids and the role of associated higher order gradient continuum models. *J. Mech. Phys. Solids* 1996; **44**(11):1891–1928.
- Tvergaard V. Studies of the micromechanics of materials. *Eur. J. Mech. A/Solids* 1997; **16**:5–24.
- Verhoosel CV, Remmers JJC, Gutierrez MA and de Borst R. Computational homogenization for adhesive and cohesive failure in quasi-brittle solids. *Int. J. Numer. Methods Eng.* 2010; **83**(8–9):1155–1179.
- Vitek V. Interatomic potentials for atomistic simulations. In *MRS Bulletin*, vol. 21, Voter AF (ed.). Materials Research Society, 1996; 20.
- Weinan E. *Principles of Multiscale Modeling*. Cambridge University Press: Cambridge, 2011.
- Weinan E, Engquist B, Lao XT, Ren WQ and Vanden-Eijnden E. Heterogeneous multiscale methods: a review. *Commun. Comput. Phys.* 2007; **2**(3):367–450.
- Wierszycki M, Szajek K, Lodygowski T and Nowak M. A two-scale approach for trabecular bone microstructure modeling based on computational homogenization procedure. *Comput. Mech.* 2014; **54**(2):287–298.
- Wilde RE and Singh S. *Statistical Mechanics, Fundamentals and Modern Applications*. John Wiley & Sons, Inc.: New York, 1998.
- Willis JR. Bounds on self-consistent estimates for the overall properties of anisotropic composites. *J. Mech. Phys. Solids* 1977; **25**:185–202.
- Willis JR. Upper and lower bounds for nonlinear composite behaviour. *Mater. Sci. Eng.* 1994; **A175**:7–14.
- Yang Y, Ma FY, Lei CH, Liu YY and Li JY. Nonlinear asymptotic homogenization and the effective behavior of layered thermoelectric composites. *J. Mech. Phys. Solids* 2013; **61**(8):1768–1783.
- Yeong CLY and Torquato S. Reconstructing random media. *Phys. Rev. E* 1998; **57**(1):495–506.
- Yuan Z, Jiang T, Fish J and Morscher G. Reduced-order multiscale-multiphysics model for heterogeneous materials. *Int. J. Multiscale Comput. Eng.* 2014; **12**(1):45–64.
- Yvonnet J and He Q-C. The reduced model multiscale method (R3M) for the nonlinear homogenization of hyperelastic media at finite strain. *J. Comput. Phys.* 2007; **223**:341–368.
- Yvonnet J, Gonzalez D and He Q-C. Numerically explicit potentials for the homogenization of nonlinear elastic heterogeneous materials. *Comput. Methods Appl. Mech. Eng.* 2009; **198**:2723–2737.
- Yvonnet J, Monteiro E and He QC. Computational homogenization method and reduced database model for hyperelastic heterogeneous structures. *Int. J. Multiscale Comput. Eng.* 2013; **11**(3):201–225.
- Zäh D and Miehe C. Computational homogenization in dissipative electro-mechanics of functional materials. *Comput. Methods Appl. Mech. Eng.* 2013; **267**:487–510.
- Zaoui A. Continuum micromechanics: survey. *J. Eng. Mech.* 2002; **128**(8):808–816.

Zaoui A and Masson R. Micromechanics based modelling of plastic polycrystals: an affine formulation. *Mater. Sci. Eng.* 2000; **A285**:418–424.

Zeman J and Šejnoha M. From random microstructures to representative volume elements. *Modell. Simul. Mater. Sci. Eng.* 2007; **15**(4):S325–S335.

Zhuang XY, Wang Q and Zhu HH. A 3D computational homogenization model for porous material and parameters identification. *Comput. Mater. Sci.* 2015; **96**:536–548.